Scattering, Diffraction, Material Particles and Waves

C.F.Majkrzak
NIST Center for Neutron Research

Summer School, June 2008

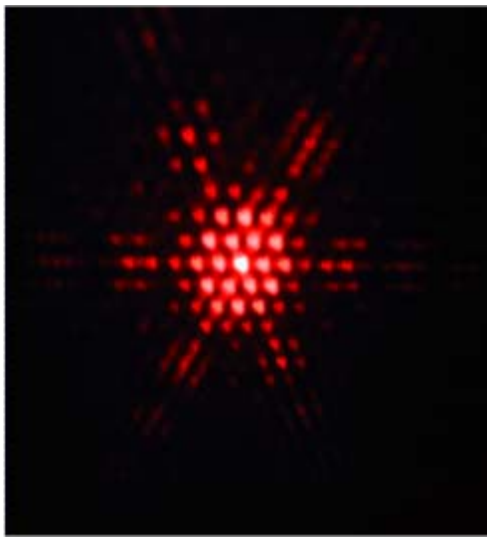

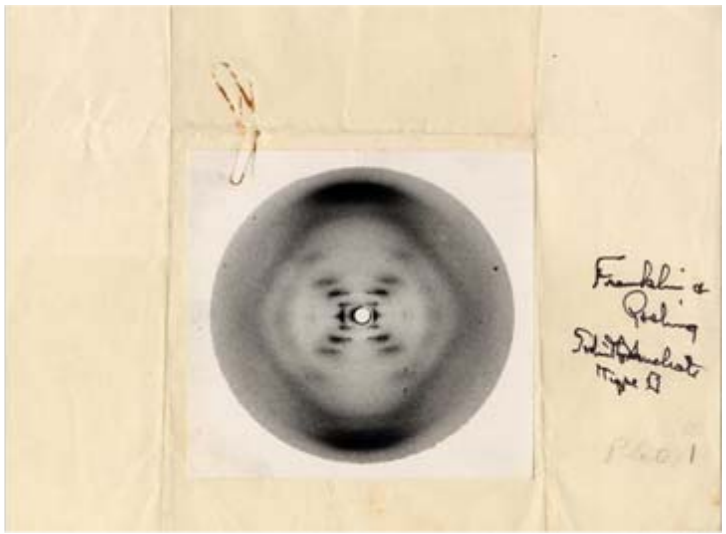

(Hexagonal aperture optical diffr. pattern – J.Newman, Union.edu) (DNA x-ray diffr. pattern - R.Franklin) (superconducting Nb vortex lattice neutron diffr. pattern – J.Lynn et al.)

X-ray transmission image.

"SPECULAR" OR "MIRROR" REFLECTION OF A WAVE

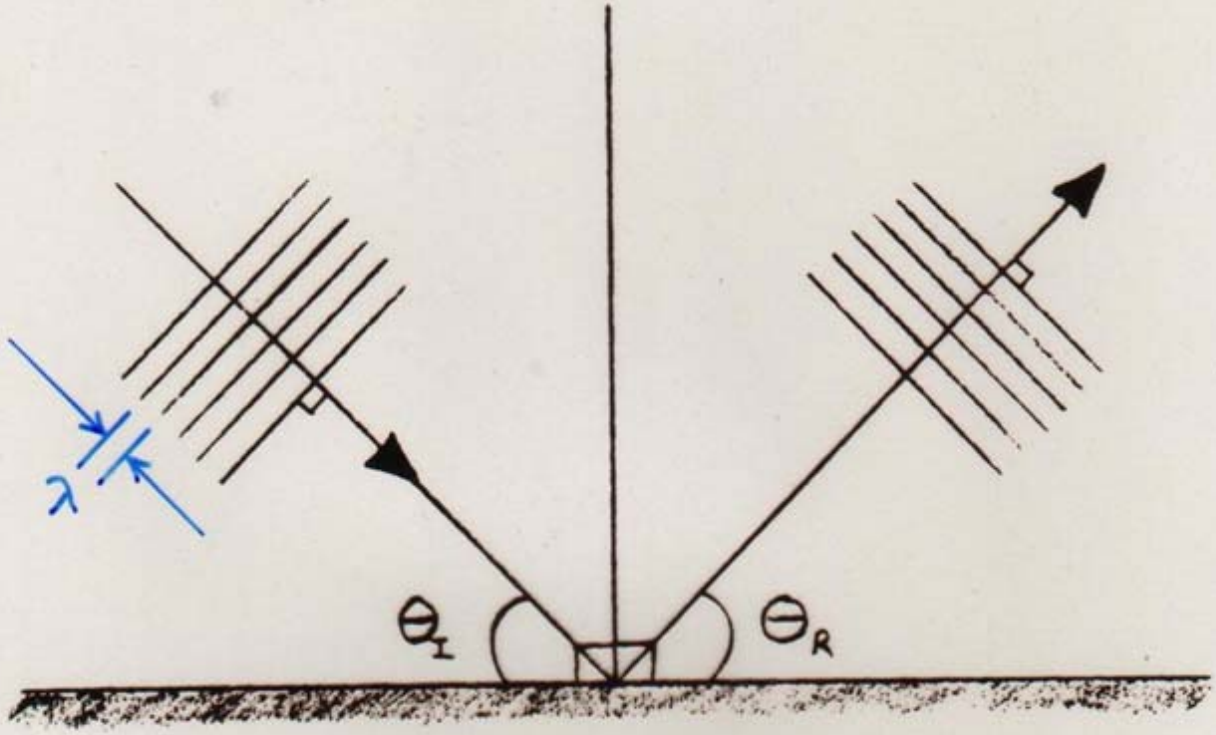

ANGLE OF INCIDENCE θ_I

= ANGLE OF REFLECTION θ_R

REFRACTION OF A LIGHT WAVE

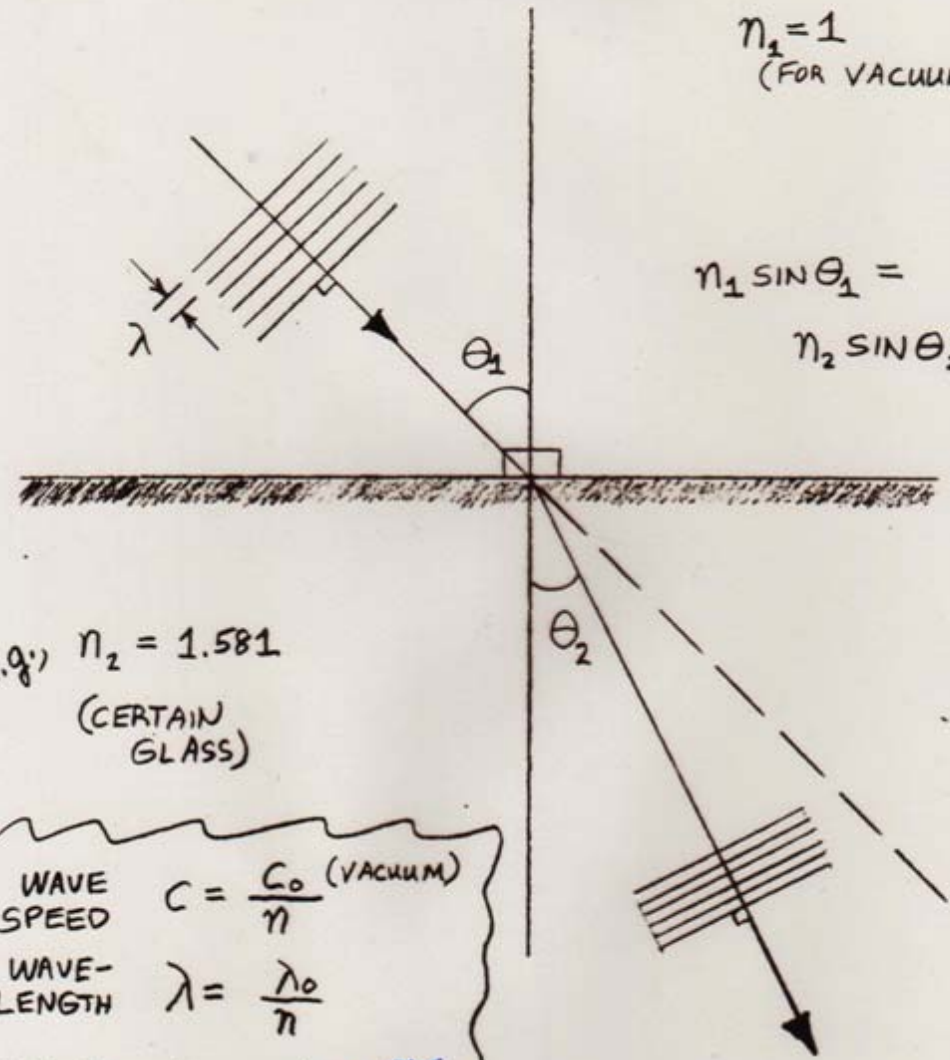

$n_1 = 1$
(FOR VACUUM)

$n_1 \sin\theta_1 = n_2 \sin\theta_2$

e.g.) $n_2 = 1.581$
(CERTAIN GLASS)

WAVE SPEED	$c = \frac{c_0}{n}$ (VACUUM)
WAVE-LENGTH	$\lambda = \frac{\lambda_0}{n}$
WAVE-VECTOR	$k = n k_0 = \frac{2\pi\nu}{c}$
FREQUENCY	ν = CONSTANT

REFRACTIVE INDEX n DEPENDS ON MATERIAL AND WAVELENGTH OF THE LIGHT

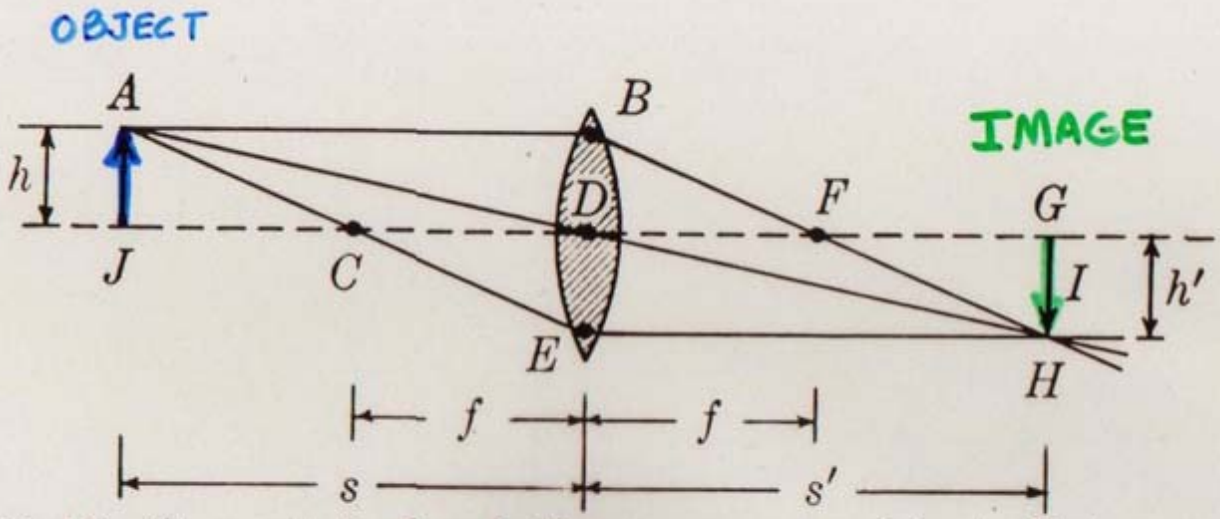

Figure 44-10. Geometrical relations among object distance s, image distance s', and focal length f.
(from Weidner & Sells, Elementary Classical Physics)

$$\boxed{1/f = 1/s + 1/s'}$$

$$h/s = h'/s'$$

The ratio of image-object *distances*, s'/s, is equal to the ratio of in object *sizes*, h'/h. This ratio h'/h is known as the *lateral magnification*.

Angularly divergent white light source.

Angularly collimated white beam.

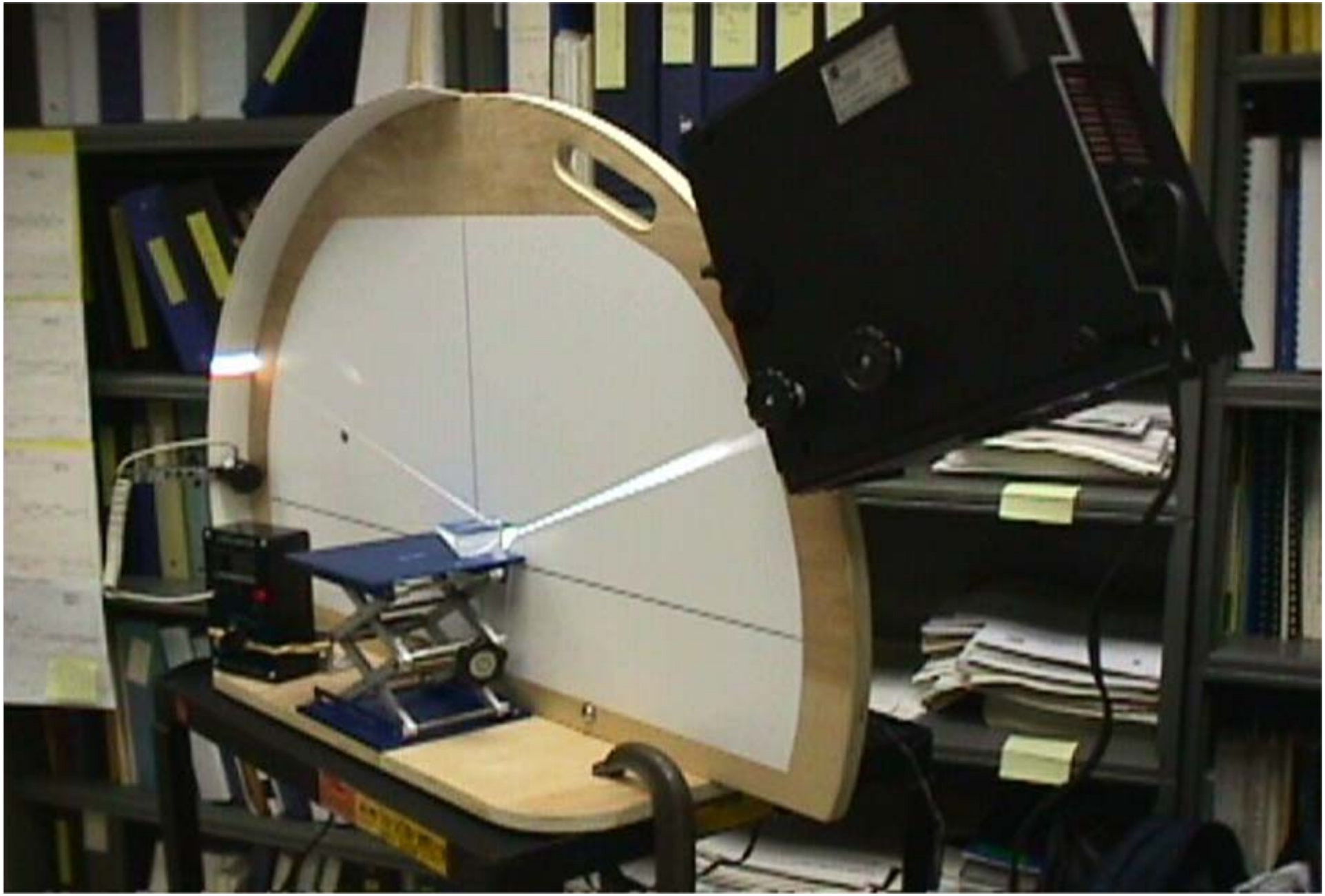

Collimated white beam specularly reflected.

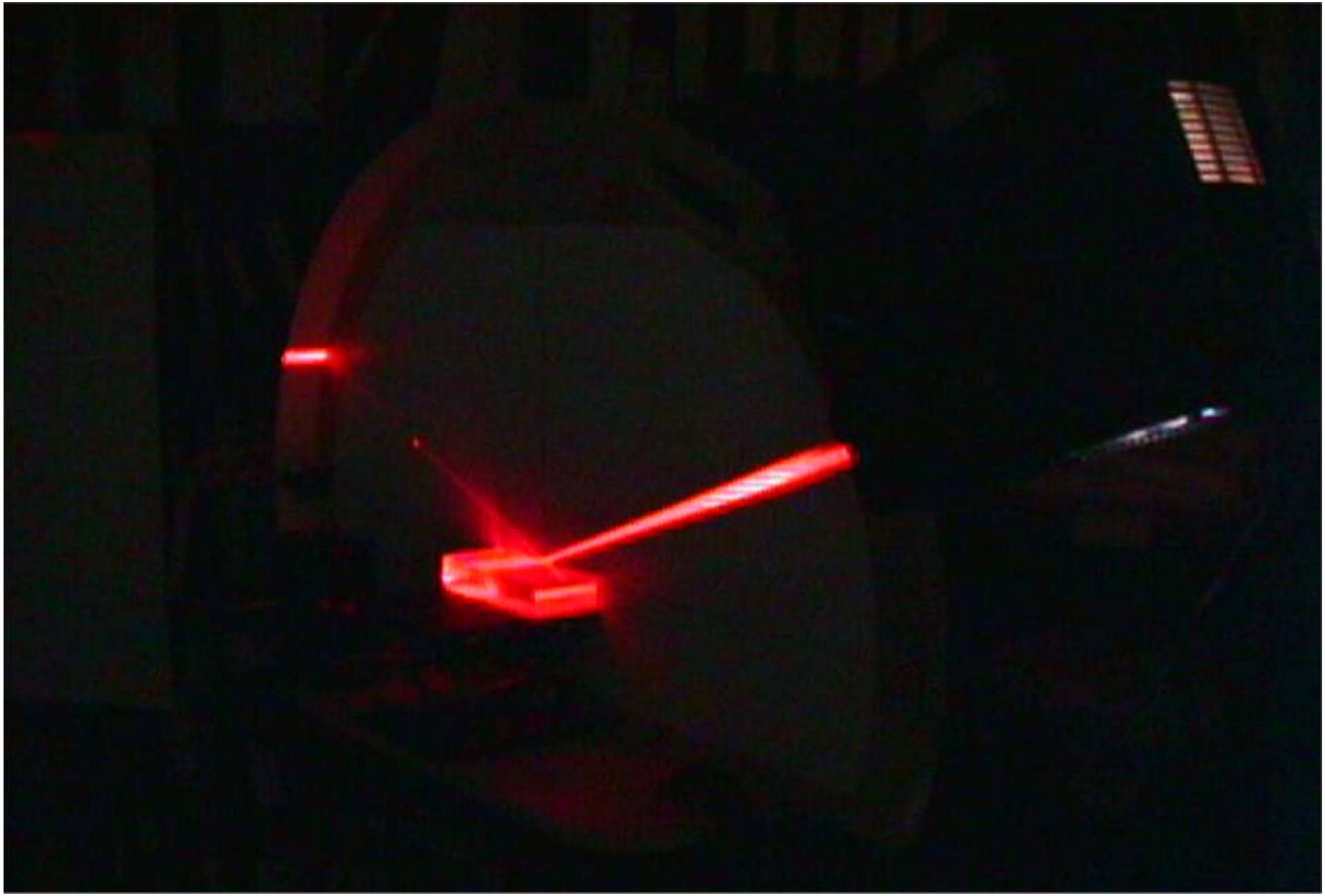

Monochromatic, collimated beam specularly reflected.

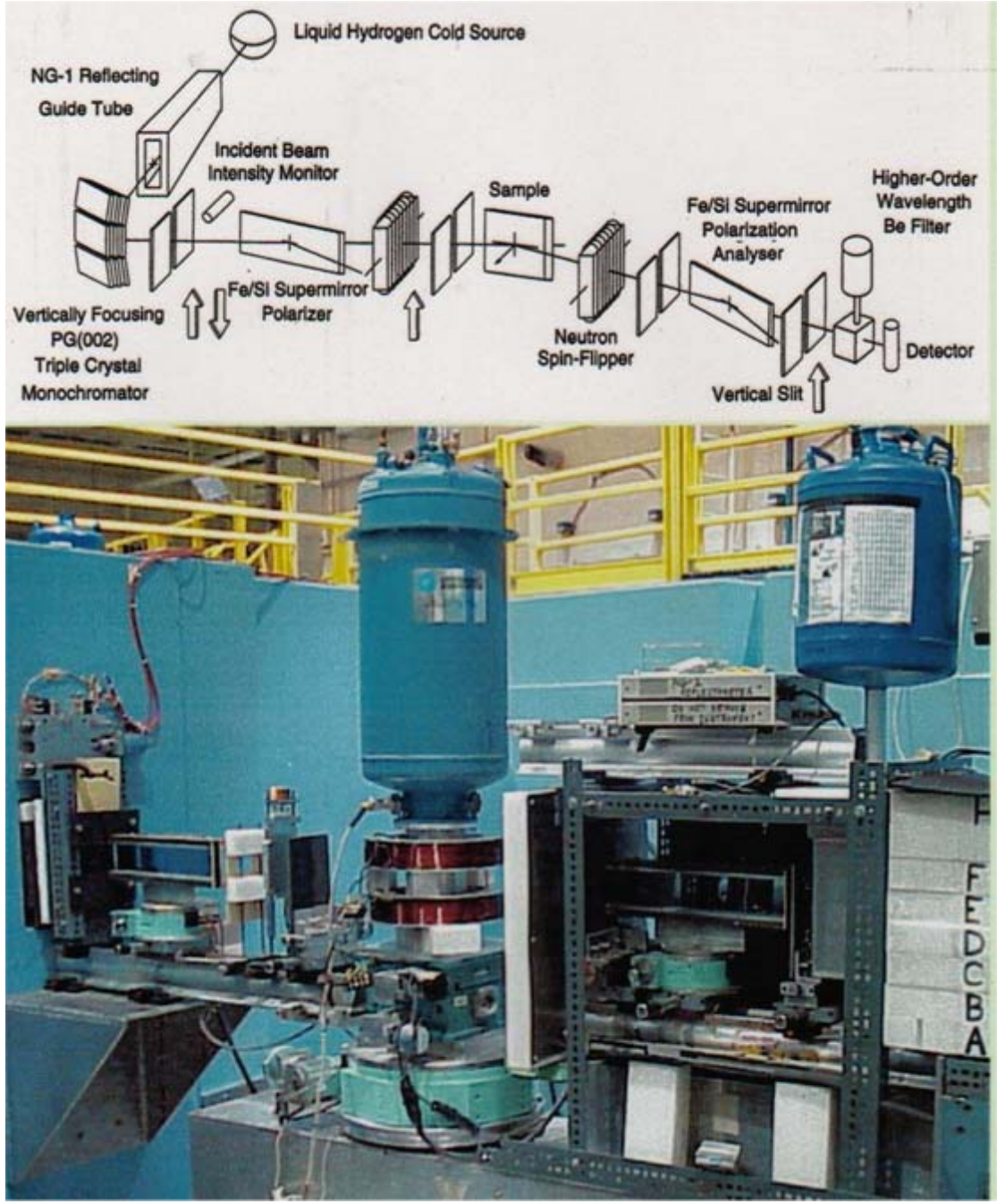

Polarized neutron reflectometer/diffractometer at the NIST Center for Neutron Research.

Flea head, 170 x magnification, scanning electron microscope, www.uq.edu.au (University of Queensland, Australia, Center for Microscopy and Microanalysis).

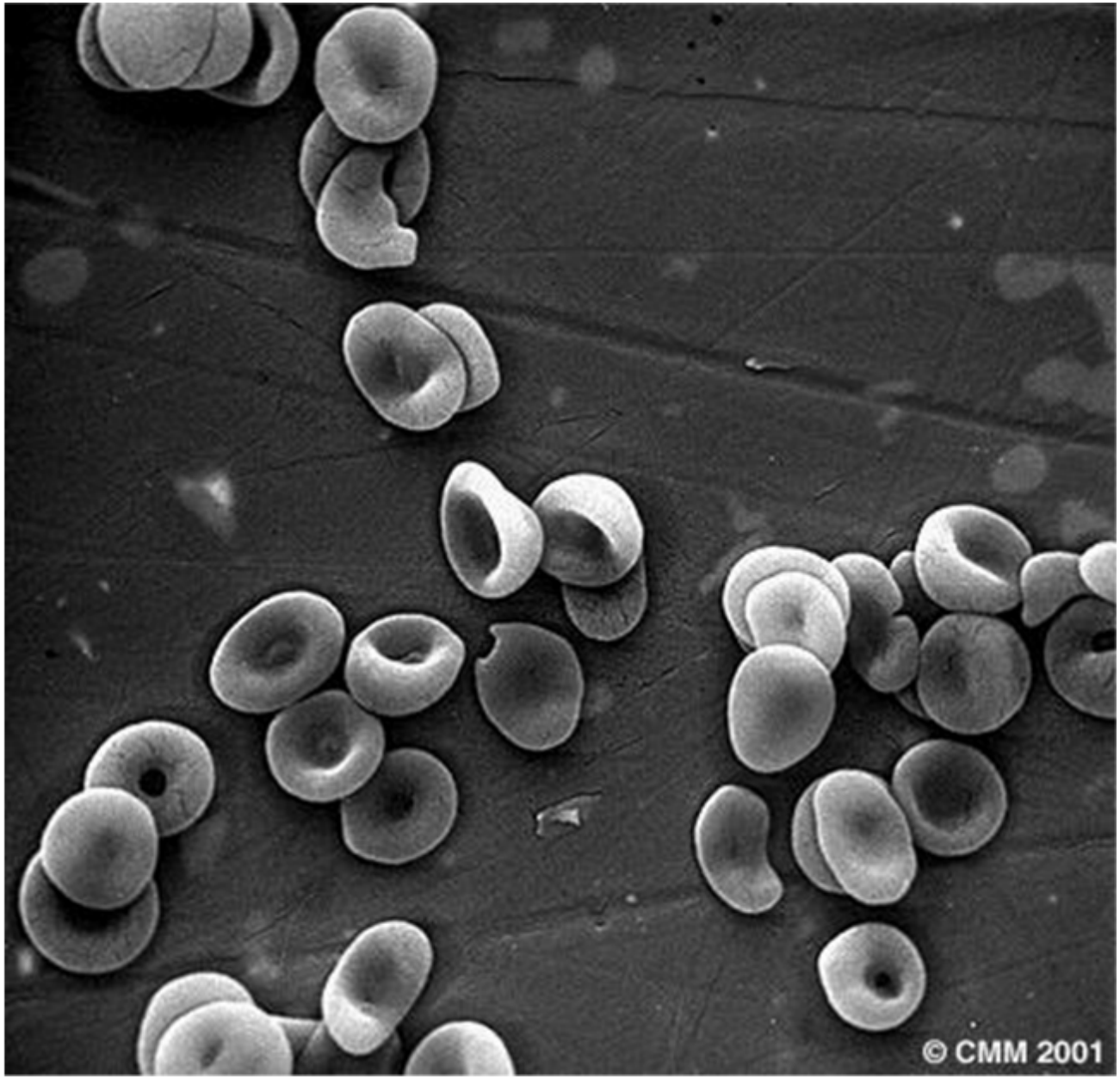

Blood cells, 2000 x magnification, scanning electron microscope, www.uq.edu.au.

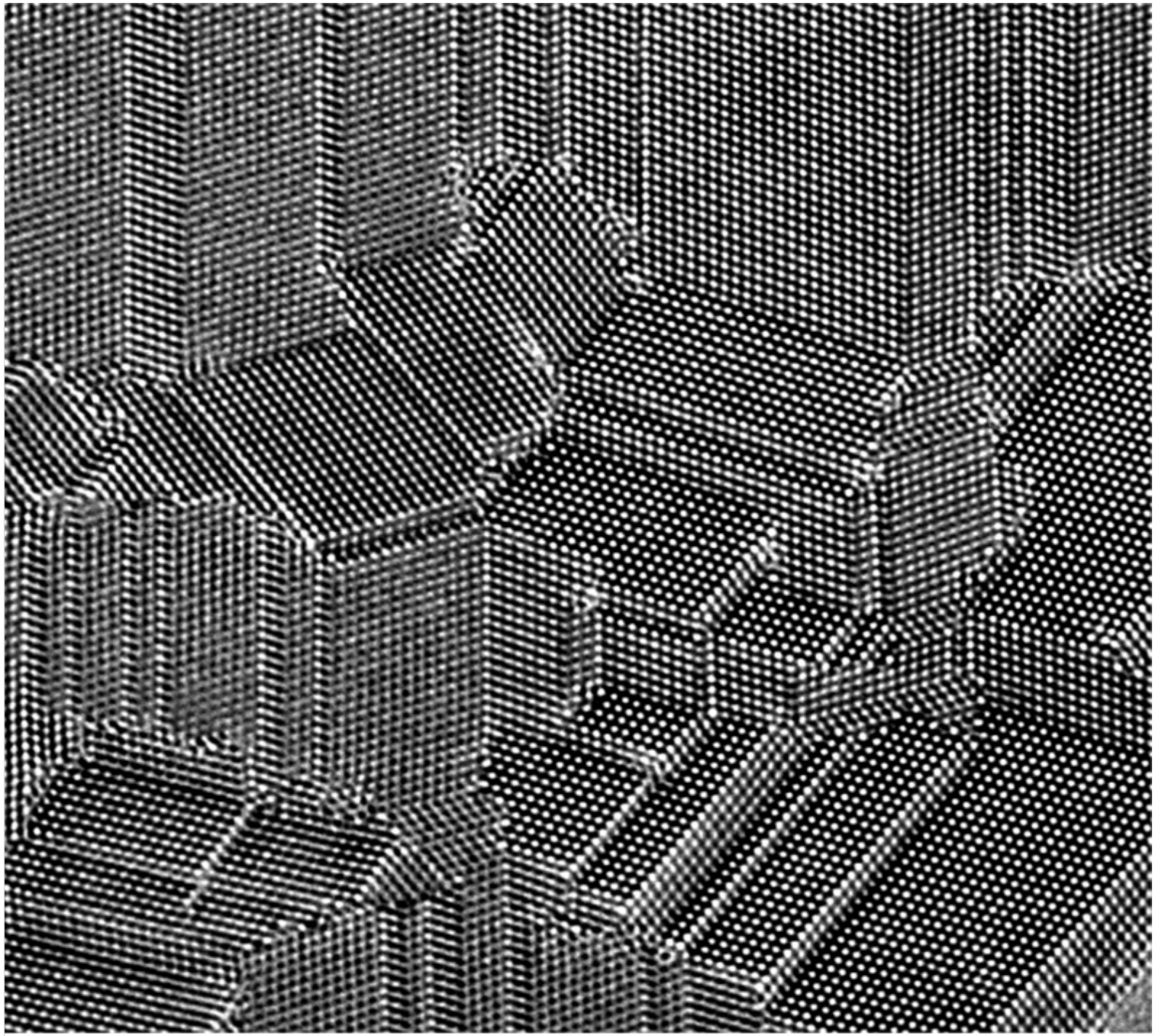

Atomic resolution micrograph of multiply-twinned nanocrystalline film of Si. (C. Song)

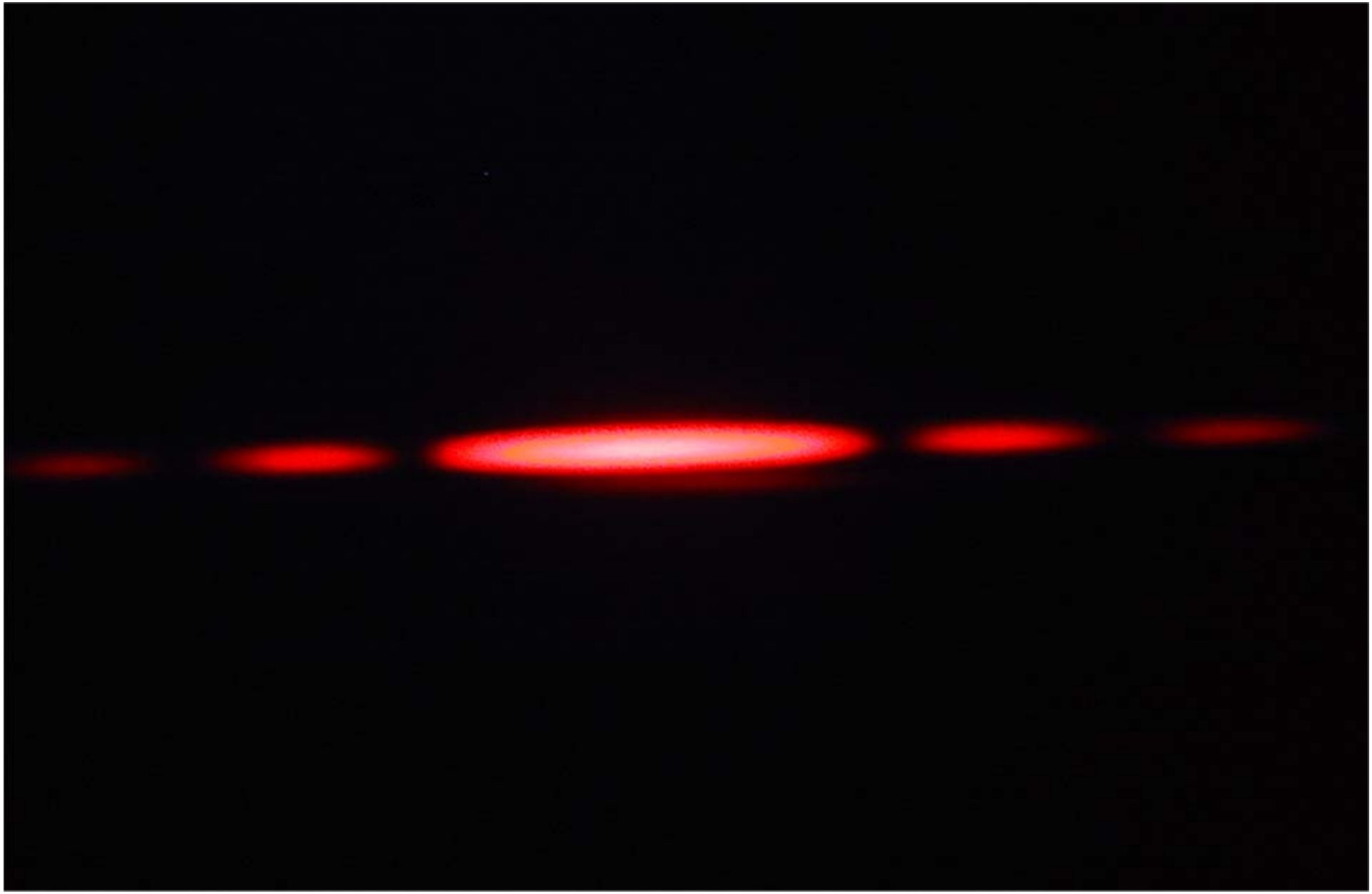

Single slit monochromatic light diffraction – Maleki/Newman at www1.union.edu.

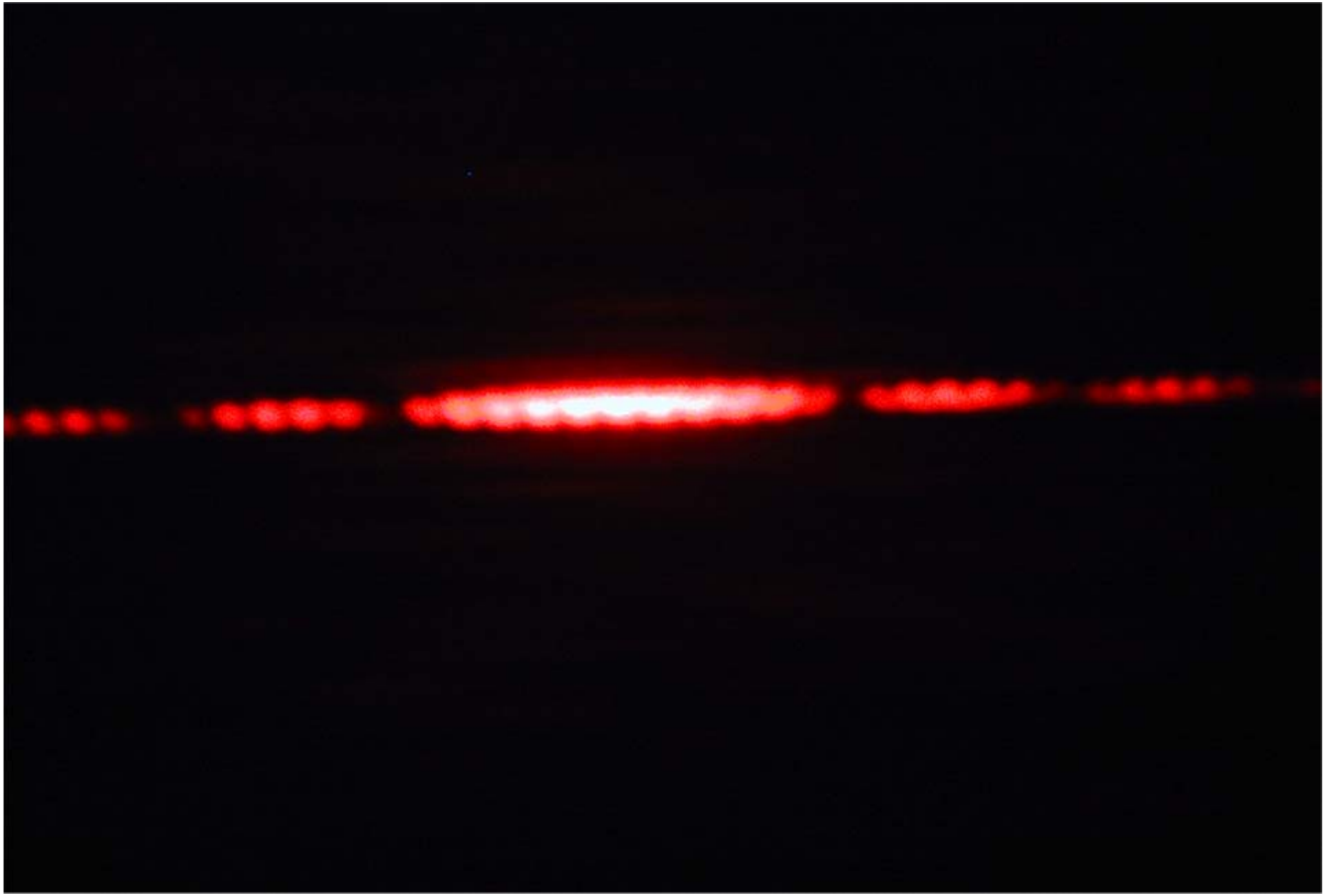

Double slit monochromatic light diffraction – Maleki/Newman at www1.union.edu.

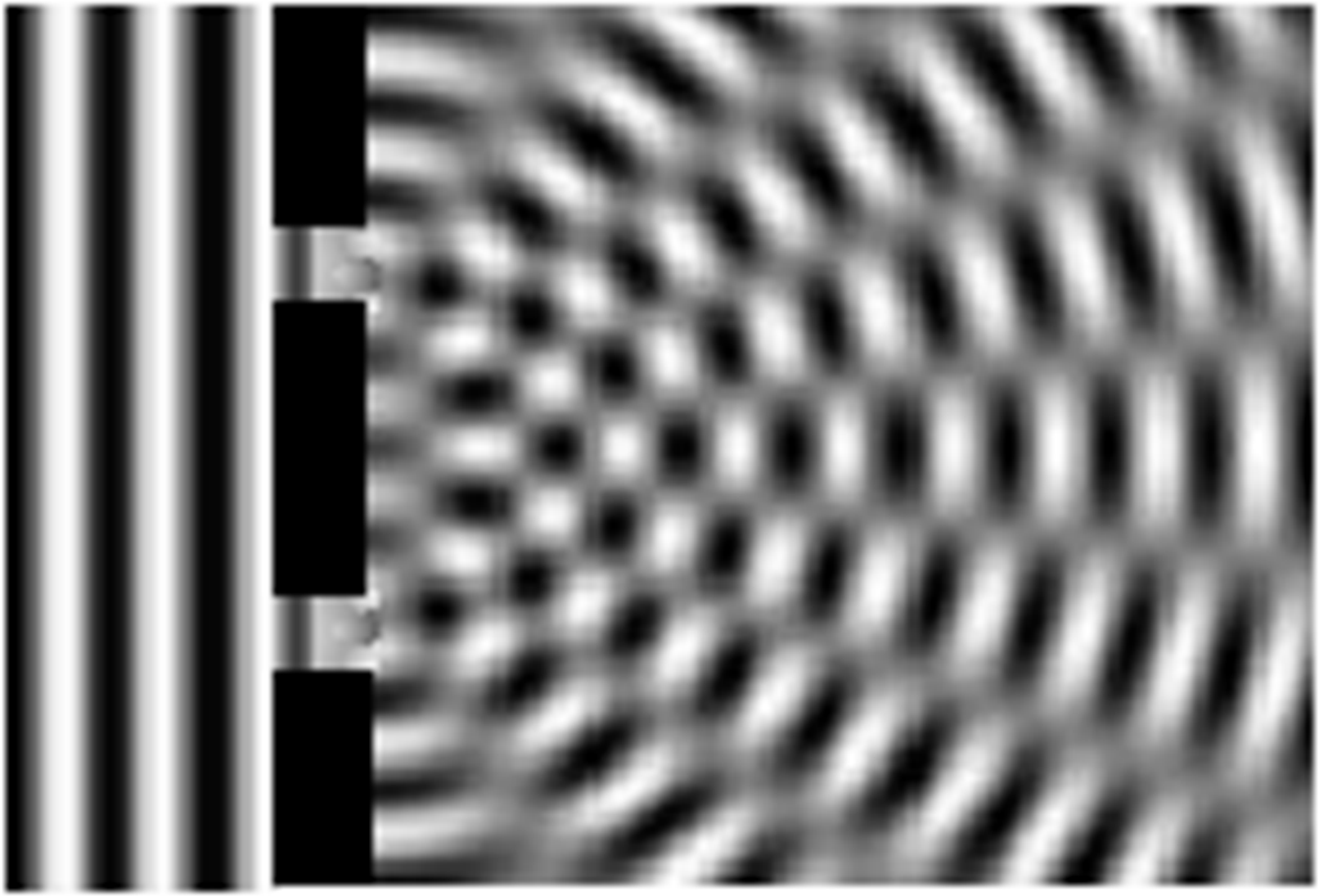

Water wave diffracting through a double aperture (from left to right) – B.Crowell, *Light and Matter*, www.vias.org/physics.

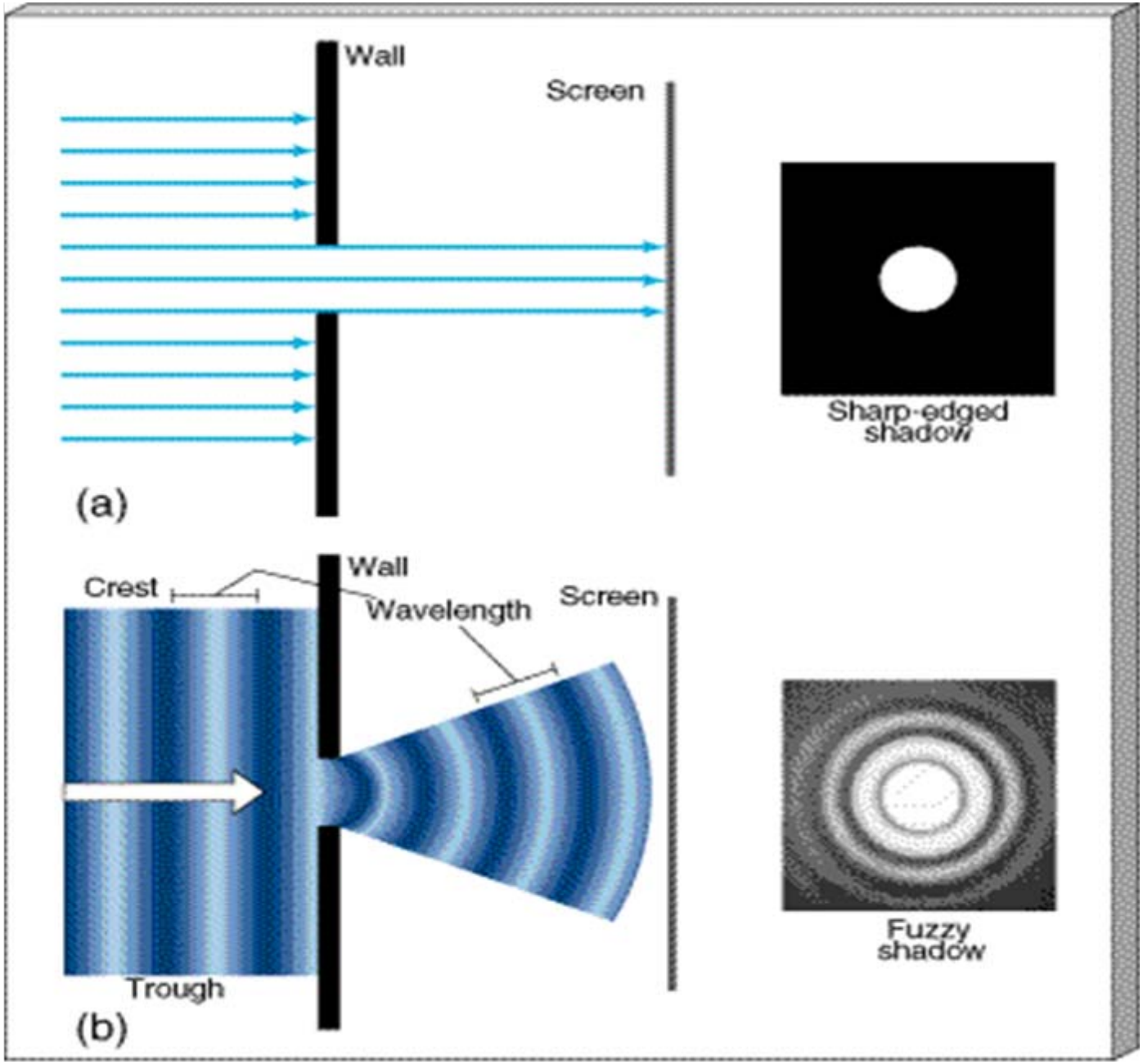

(physics.fortlewis.edu)

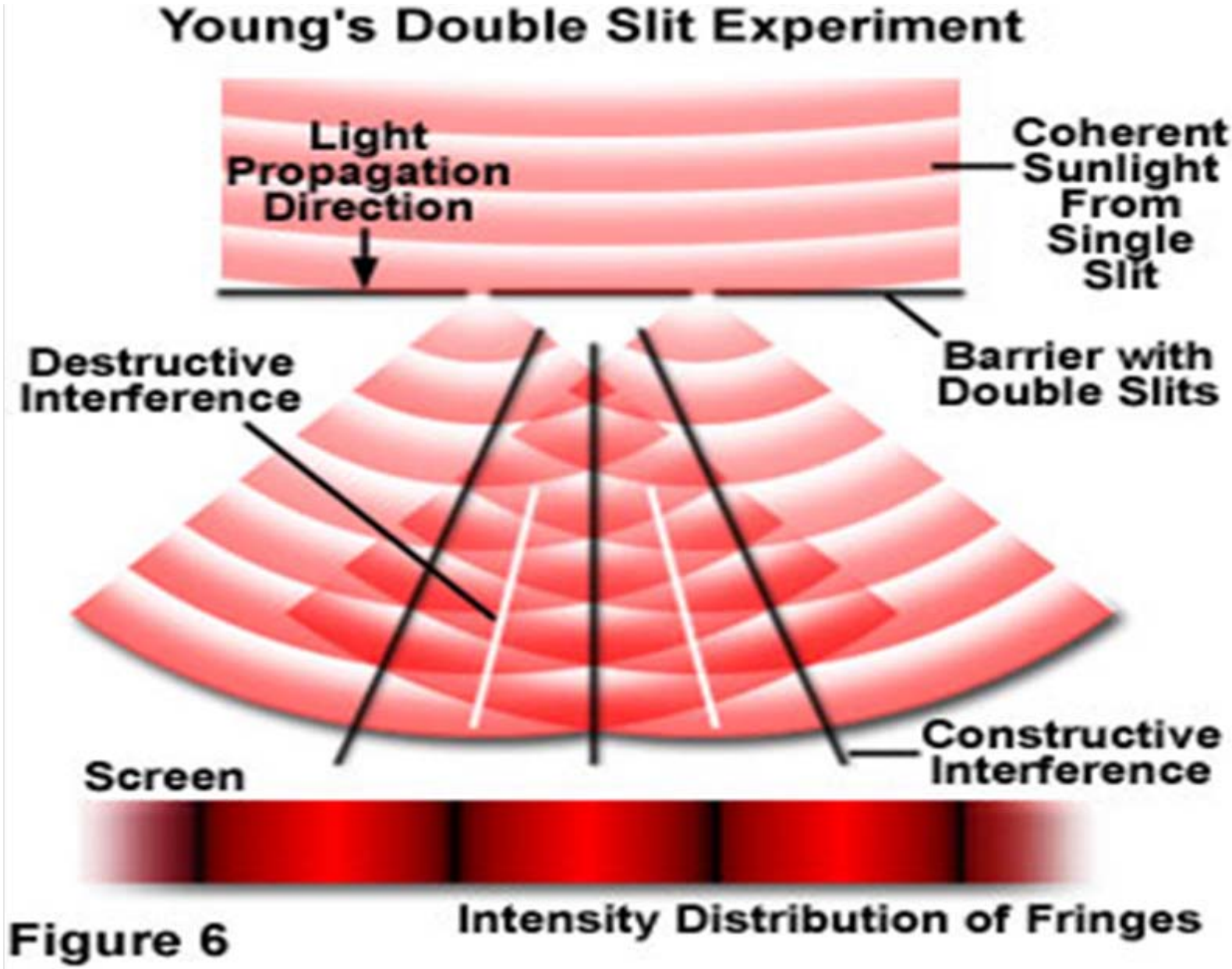

M.W.Davidson and M.Abramowitz, micro.magnet.fsu.edu.

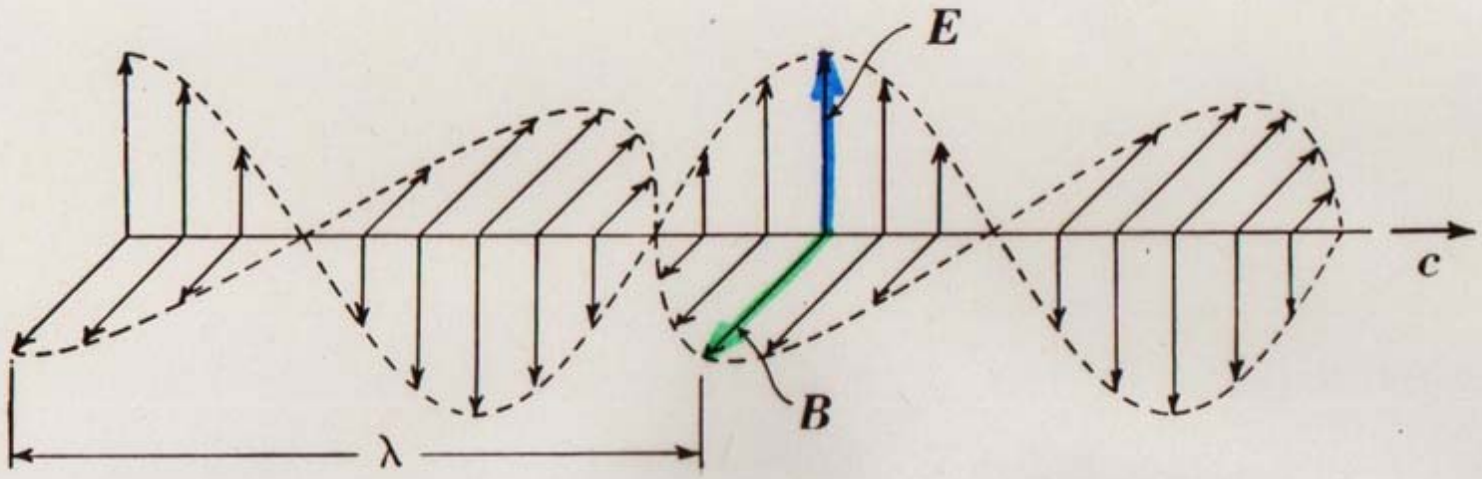

Figure 41-15. Representations of the electric and magnetic fields of a sinusoidal electromagnetic wave: (a) the field lines; (b) the sinusoidally varying amplitudes. (after Weidner & Sells, Elementary Classical Physics)

PHOTON

- ZERO MASS
- VELOCITY (IN VACUUM)

  $c_0 \cong 3 \times 10^8$ m/sec
- POLARIZED ELECTROMAGNETIC WAVE

(from Photonics by Saleh & Teich)

$D \propto \frac{1}{(2a)}$

$D \equiv \frac{\lambda}{\theta}$

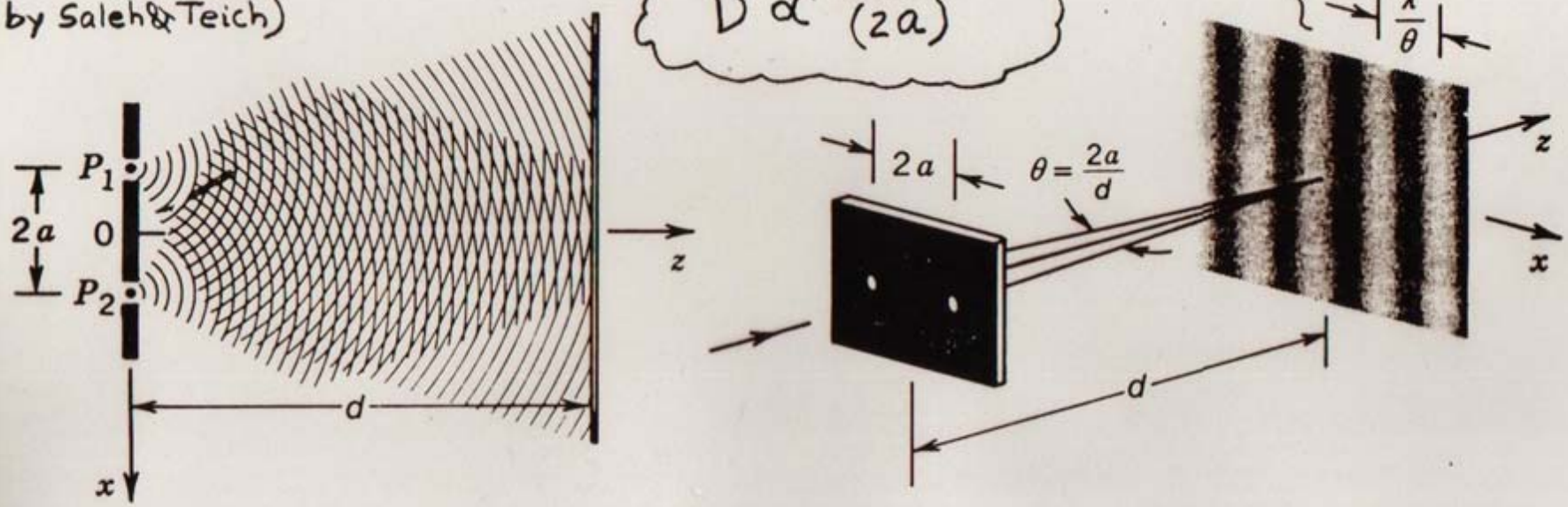

Figure 2.5-6 Interference of two spherical waves of equal intensities originating at the points P_1 and P_2. The two waves can be obtained by permitting a plane wave to impinge on two pinholes in a screen. The light intensity at an observation plane a distance d away takes the form of a sinusoidal pattern with period $\approx \lambda/\theta$.

DIFFRACTION PATTERN WHICH RESULTS FROM THE COHERENT SUPERPOSITION OF TWO WAVES (AMPLITUDES OF THE TWO WAVES ADD TOGETHER AT ANY GIVEN POINT IN SPACE)

A CHARACTERISTIC RECIPROCAL RELATIONSHIP EXISTS BETWEEN THE POSITIONS OF THE INTENSITY MAXIMA IN THE DIFFRACTION PATTERN AND THE DISTANCE SEPARATING THE OBJECTS CAUSING THE SCATTERING.

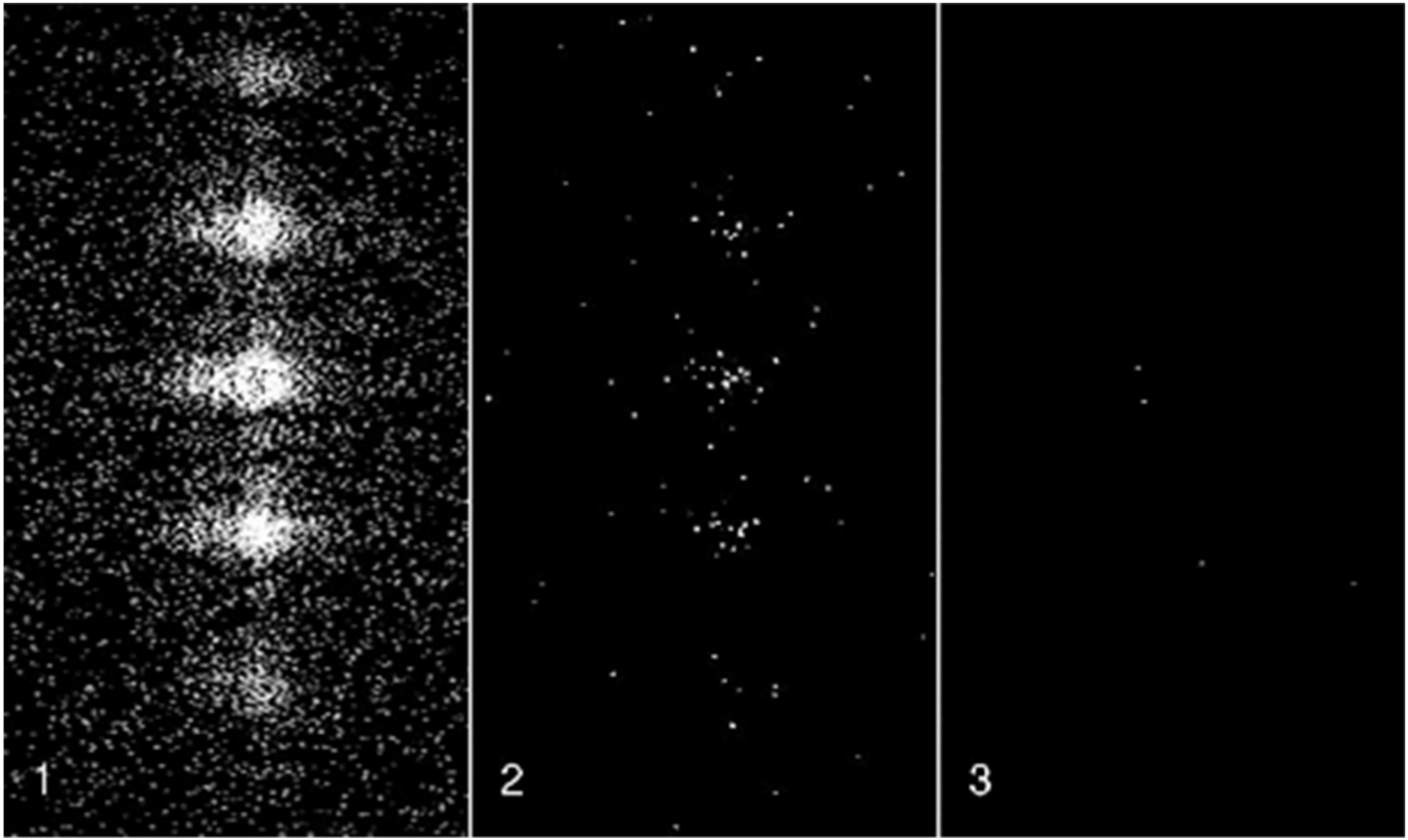

Wave interference patterns produced by monochromatic laser light diffracting through a triple slit aperture for various intensities – L.Page (www.vias.org/physics). This is a dramatic illustration of wave-particle duality.

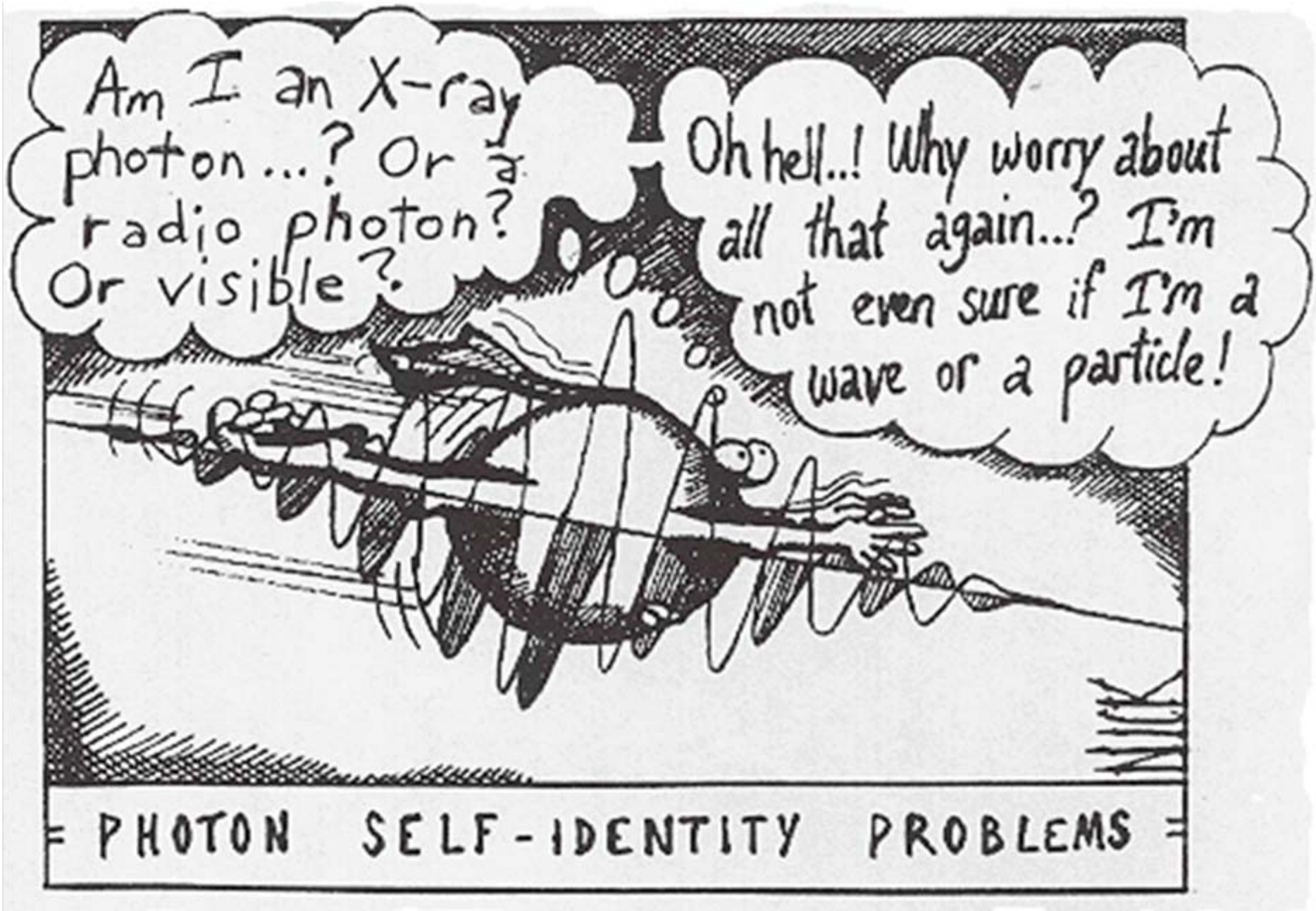

(abyss.uoregon.edu)

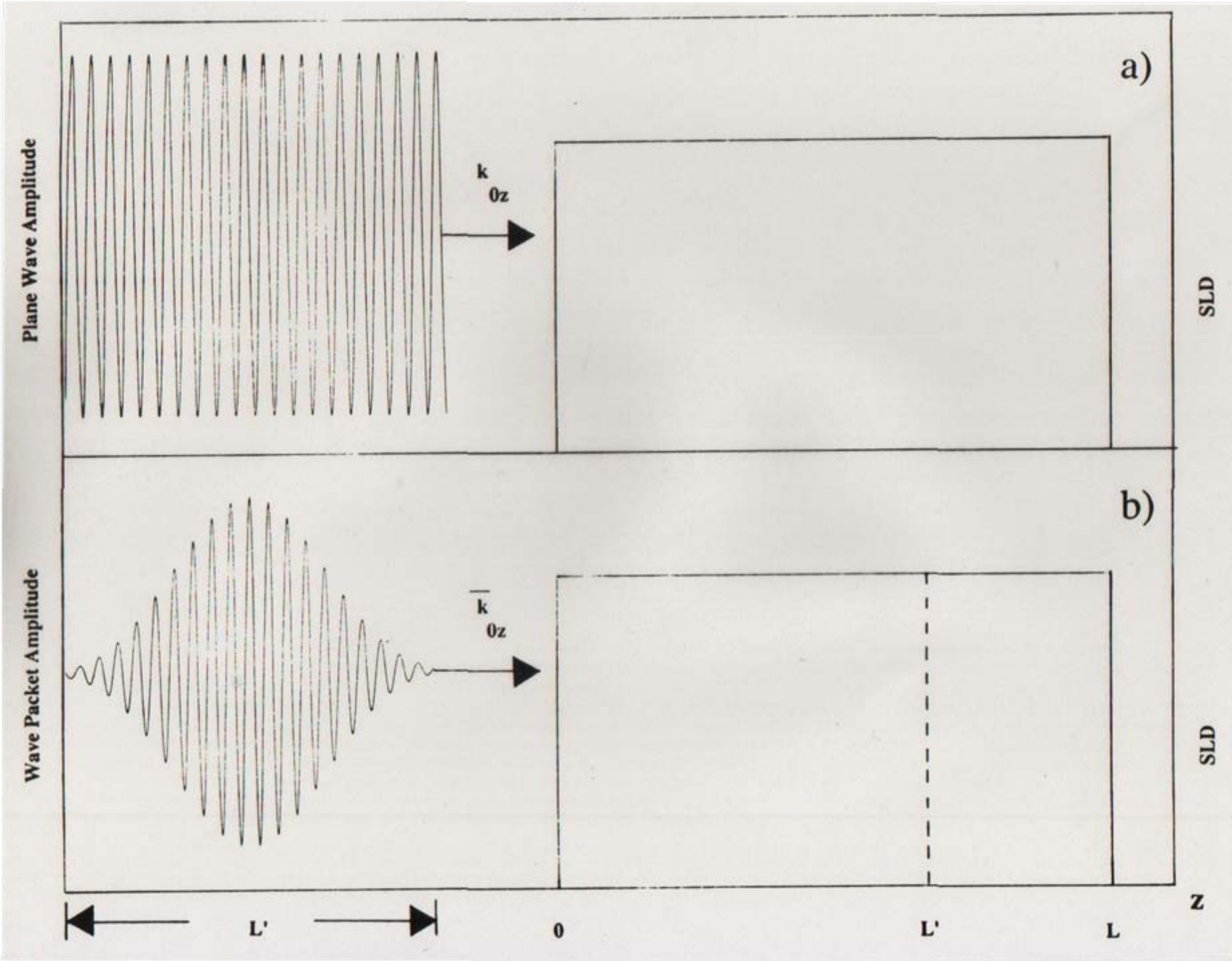
a)
Plane Wave Amplitude
k
0z
SLD
b)
Wave Packet Amplitude
k
0z
SLD
L'
0
L'
L
z

PROBES OF THE MICROSTRUCTURE OF SURFACES AND INTERFACES

photons, electrons, neutrons, atom and ion beams, miniature mechanical devices

* DIRECT IMAGING (REAL SPACE)

  e.g.:

  - optical microscopy (~ 1000 x magnification)
  - scanning electron microscopy (SEM) (orders of magnitude higher magnification than possible with light)
  - transmission electron microscopy (TEM)
  - atomic force microscopy (AFM)

* DIFFRACTION (RECIPROCAL SPACE)

  e.g.:

  - low energy electron diffraction (LEED)
  - spin polarized LEED (SPLEED)
  - reflection high energy electron diffraction (RHEED)
  - ellipsometry (optical polarimetry)
  - x-ray reflectometry
  - neutron reflectometry

For quantitative measurements of depth profiles along a normal to the surface, x-ray and neutron reflectometry are particularly useful because of their relatively weak interactions with condensed matter and the fact that these interactions can be described accurately by a comparatively simple theory. In the case of electron diffraction, on the other hand, the potential is non-local and the scattering is non-spherical, relatively strong and highly energy-dependent. For atom diffraction, the description of the interaction potential can be even more complicated.

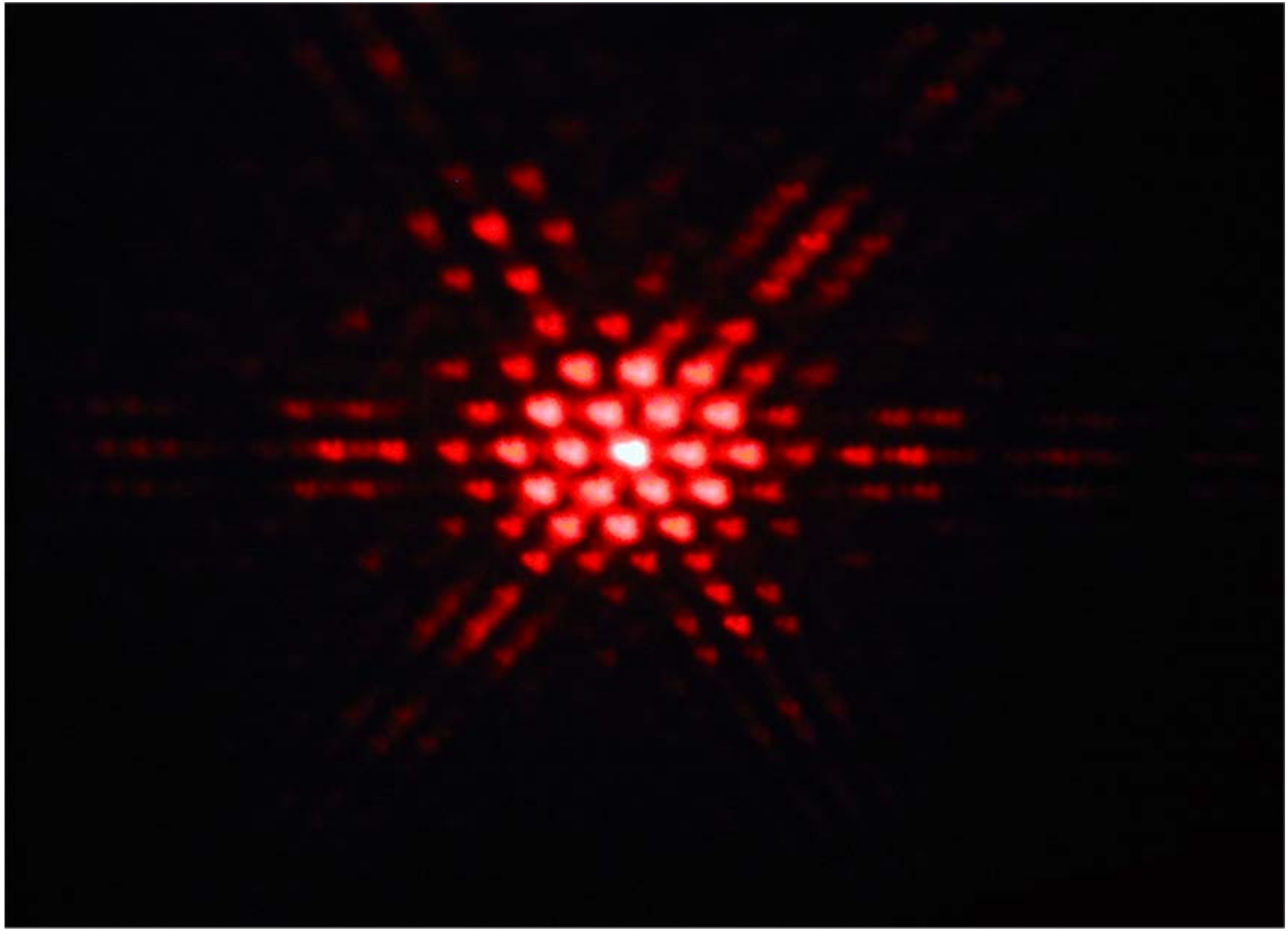

Hexagonal aperture monochromatic light diffraction – Maleki/Newman at www1.union.edu.

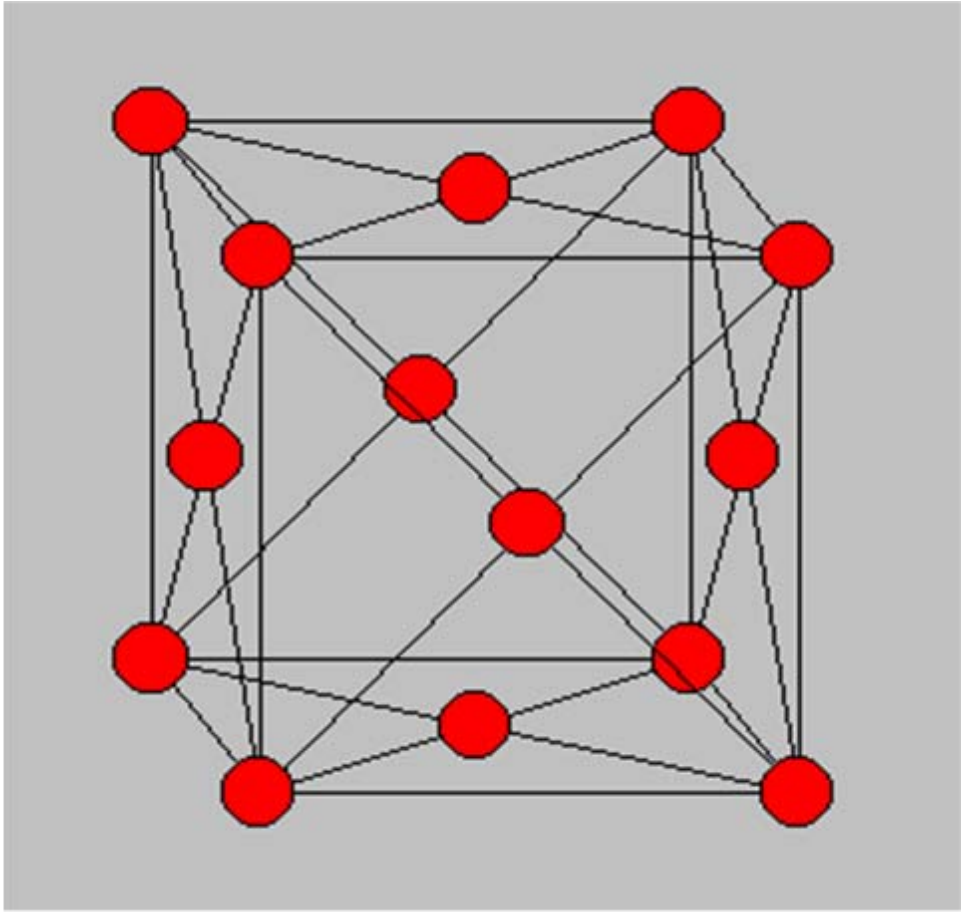

FCC aluminum crystal structure - colorado.edu.

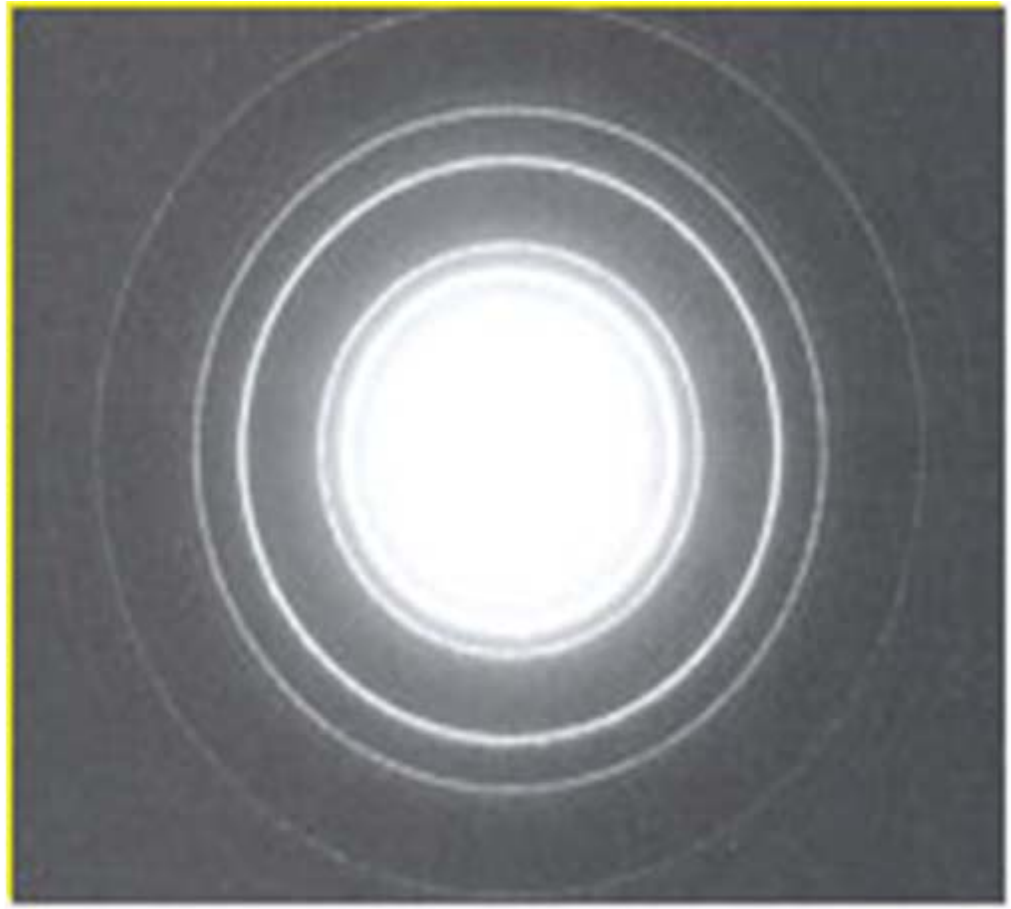

Electon diffraction pattern for aluminum - canemco.com.

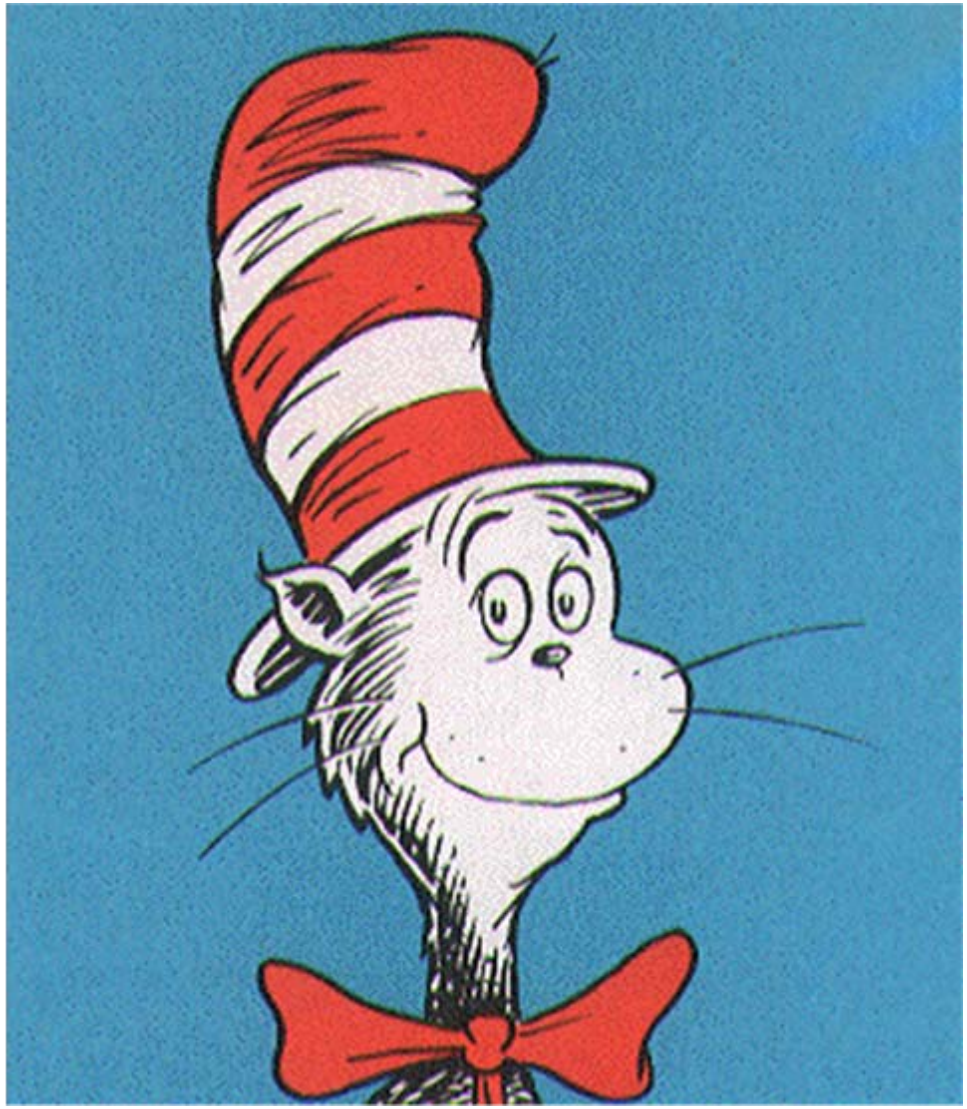

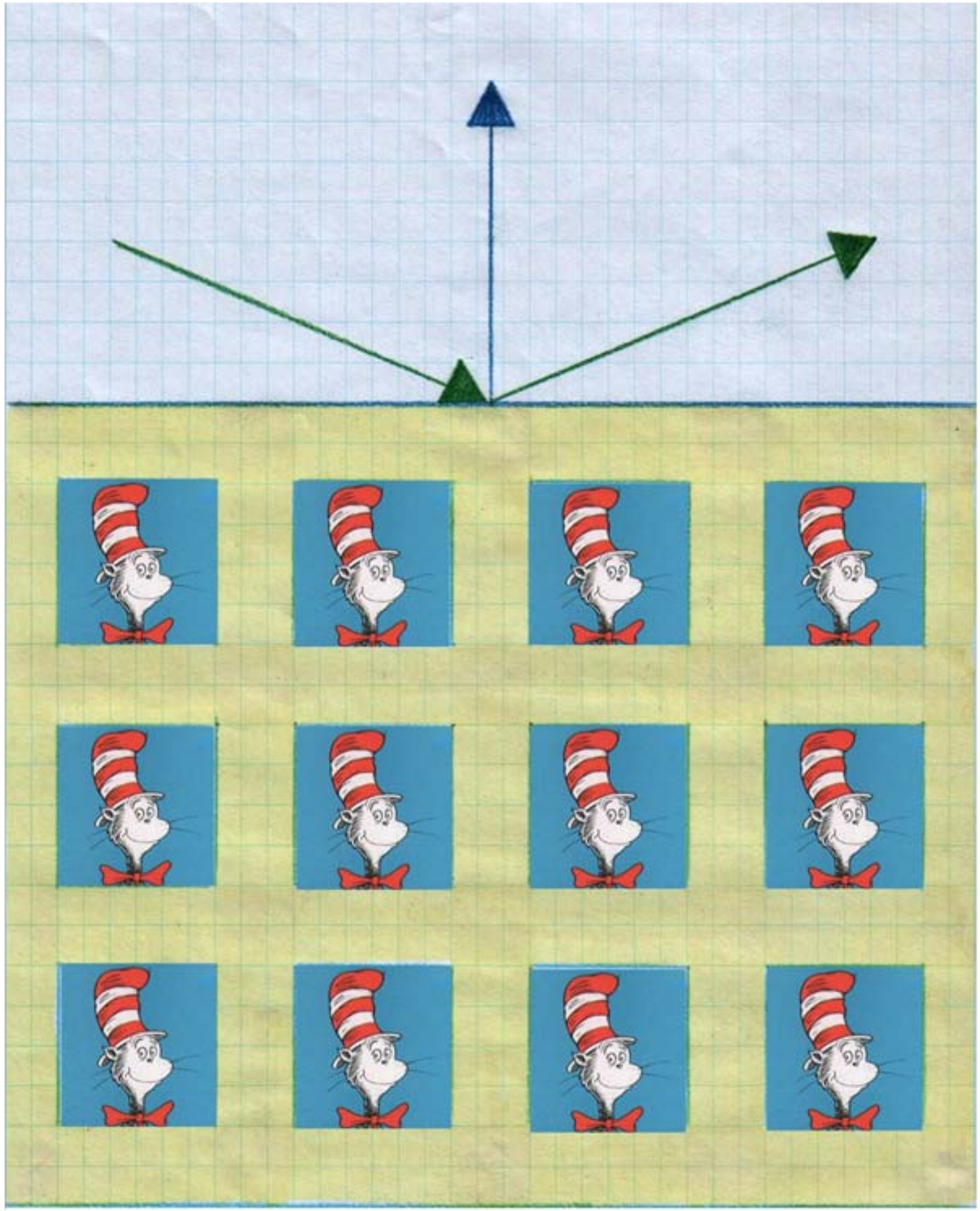

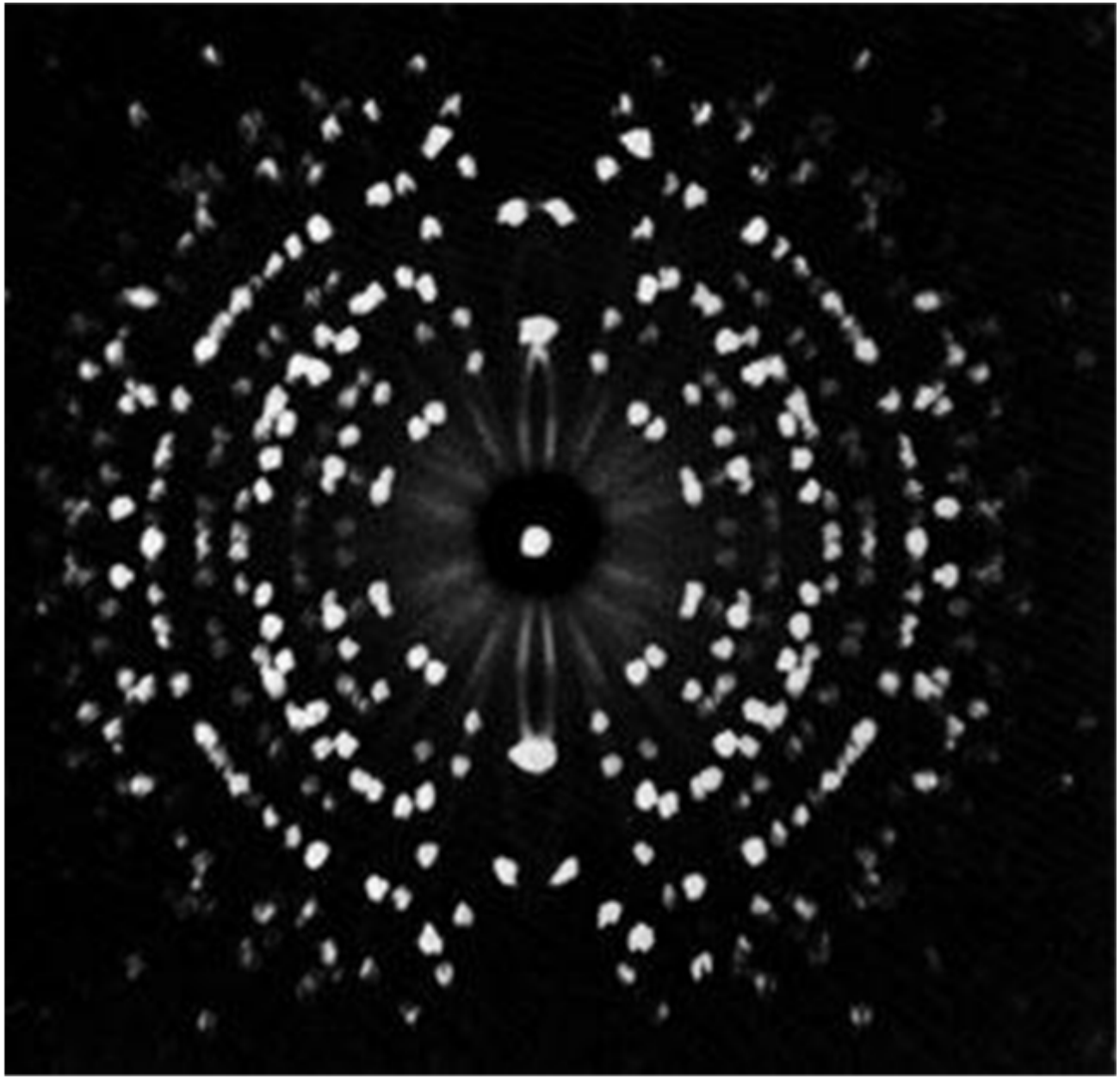

Electron diffraction pattern for a single alum crystal – H.J.Milledge, Department of Geology, University College, London.

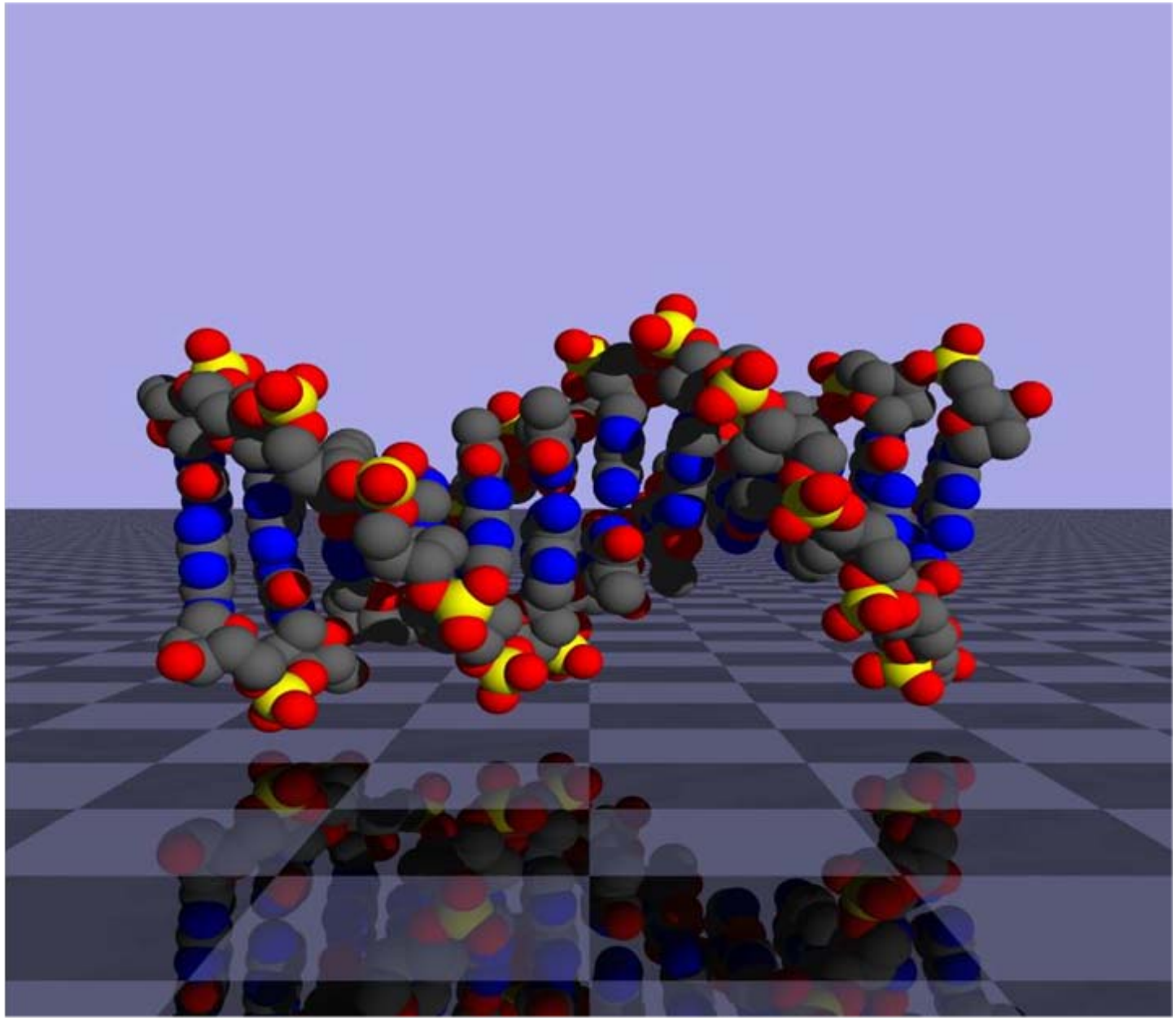

Model of DNA structure – academy.d20.co.edu.

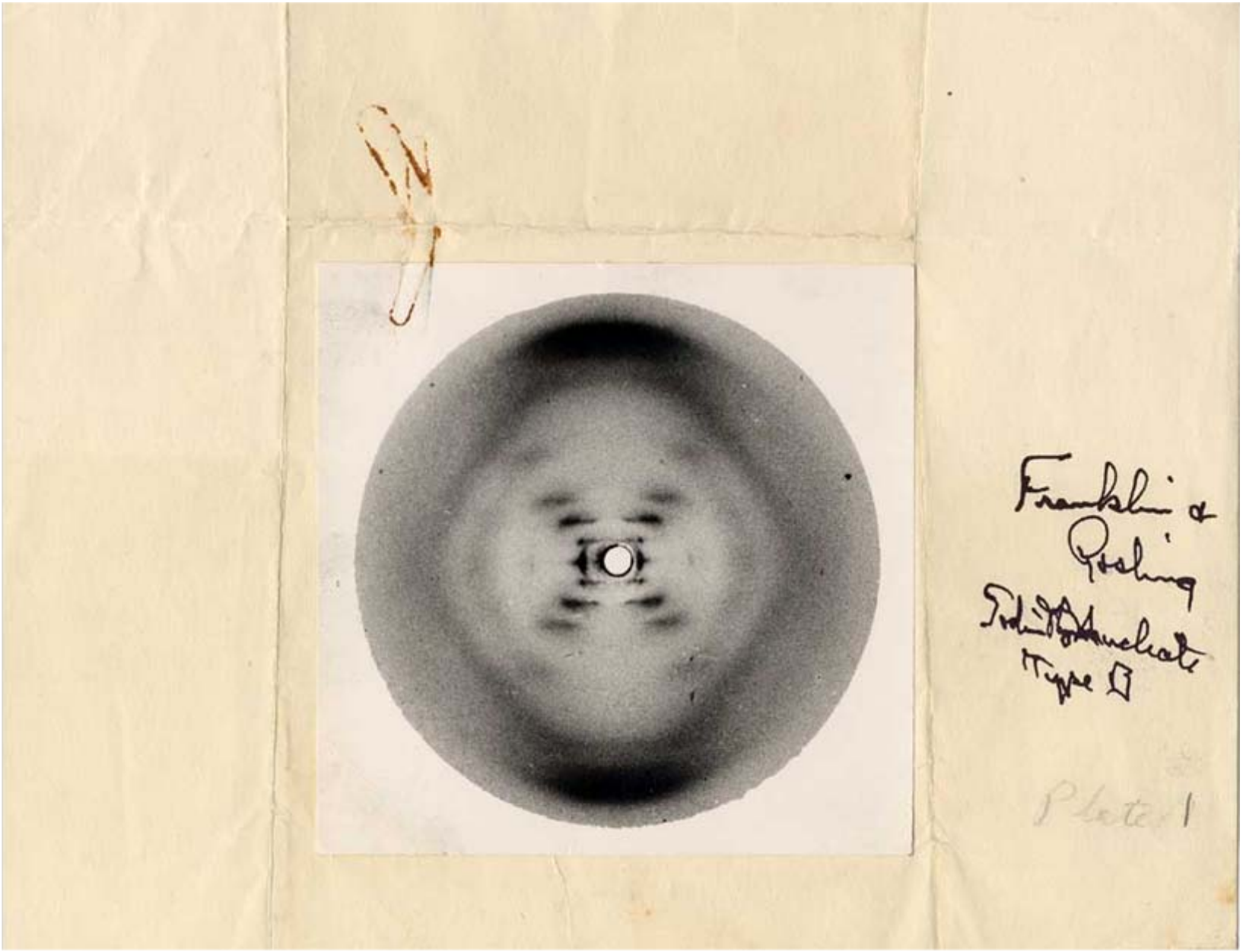

X-ray diffraction pattern for DNA obtained by Rosalind Franklin.

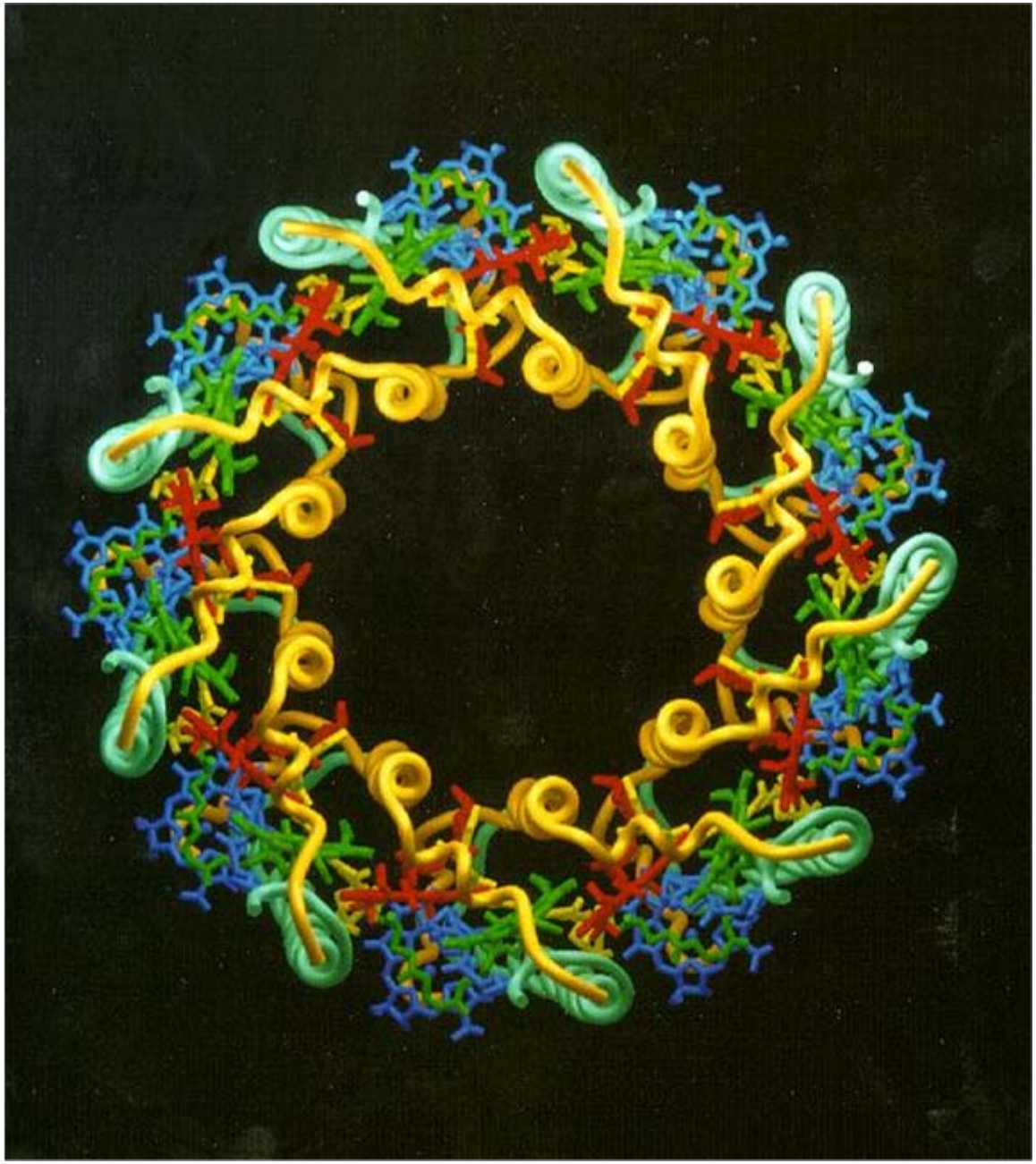

Light-harvesting protein from the bacterium *Rhodopseudomonas Acidophilla* as determined by x-ray diffraction – CCLRC Synchrotron Radiation Source, Daresbury Laboratory, UK.

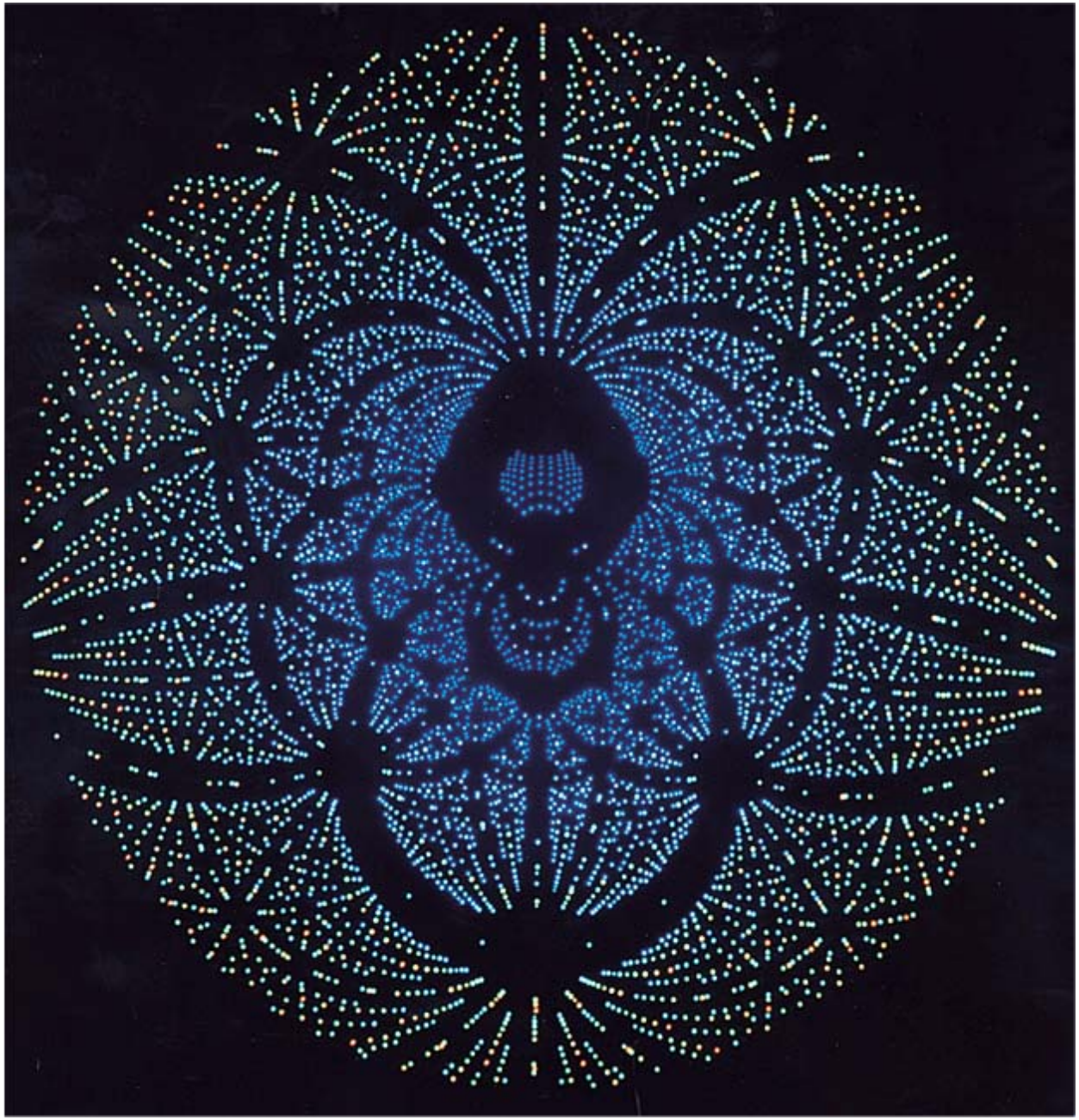

X-ray diffraction pattern from a protein found in peas – CCLRC Synchrotron Radiation Source, Daresbury Laboratory, UK.

Diblock copolymer lamellar nanostructures –
R.Jones, B.Berry, and K.Yager (NIST Polymer Division) and S.Satija, J.Dura, B.Maranville et al. (NCNR).

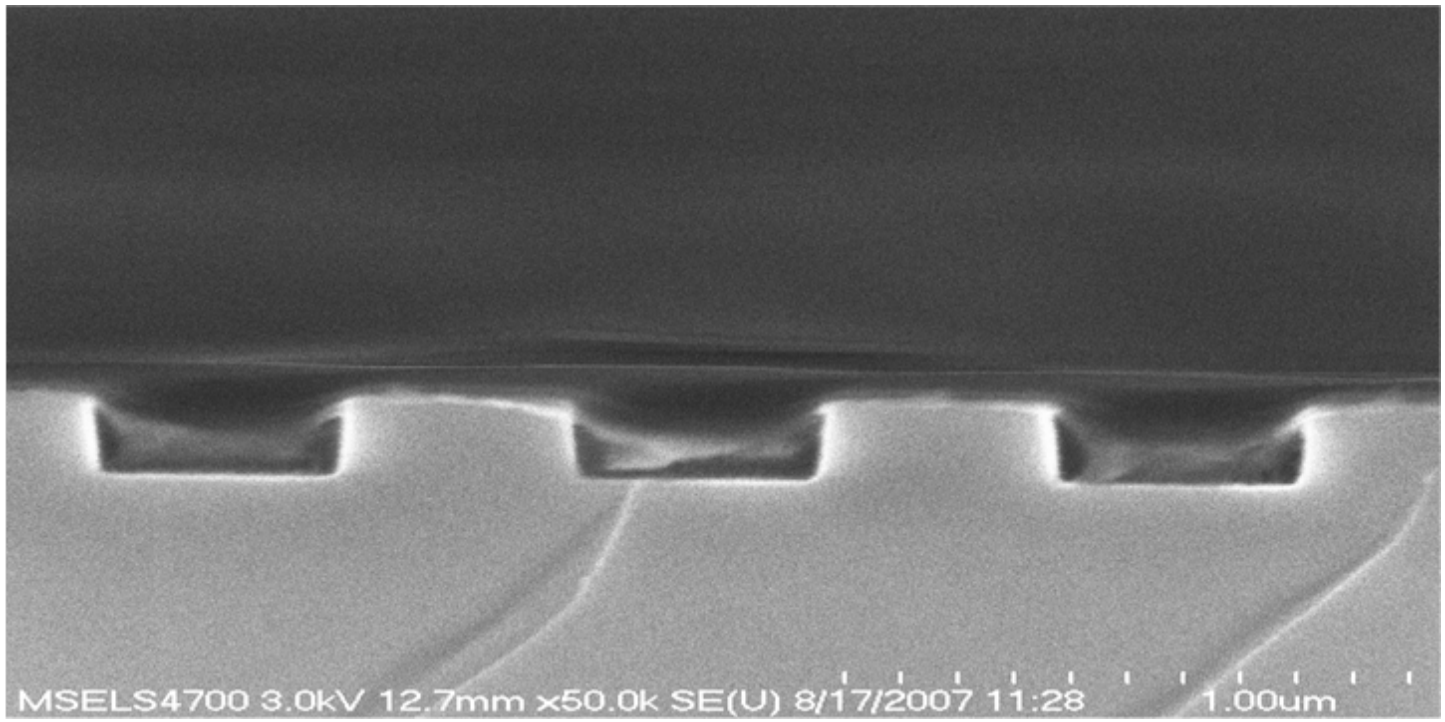

Fig 1. Side-view scanning-electron micrograph of laser-interferometry-produced silicon substrate with 400 nm channels, spaced by 400 nm for a total repeat distance of 800 nm.

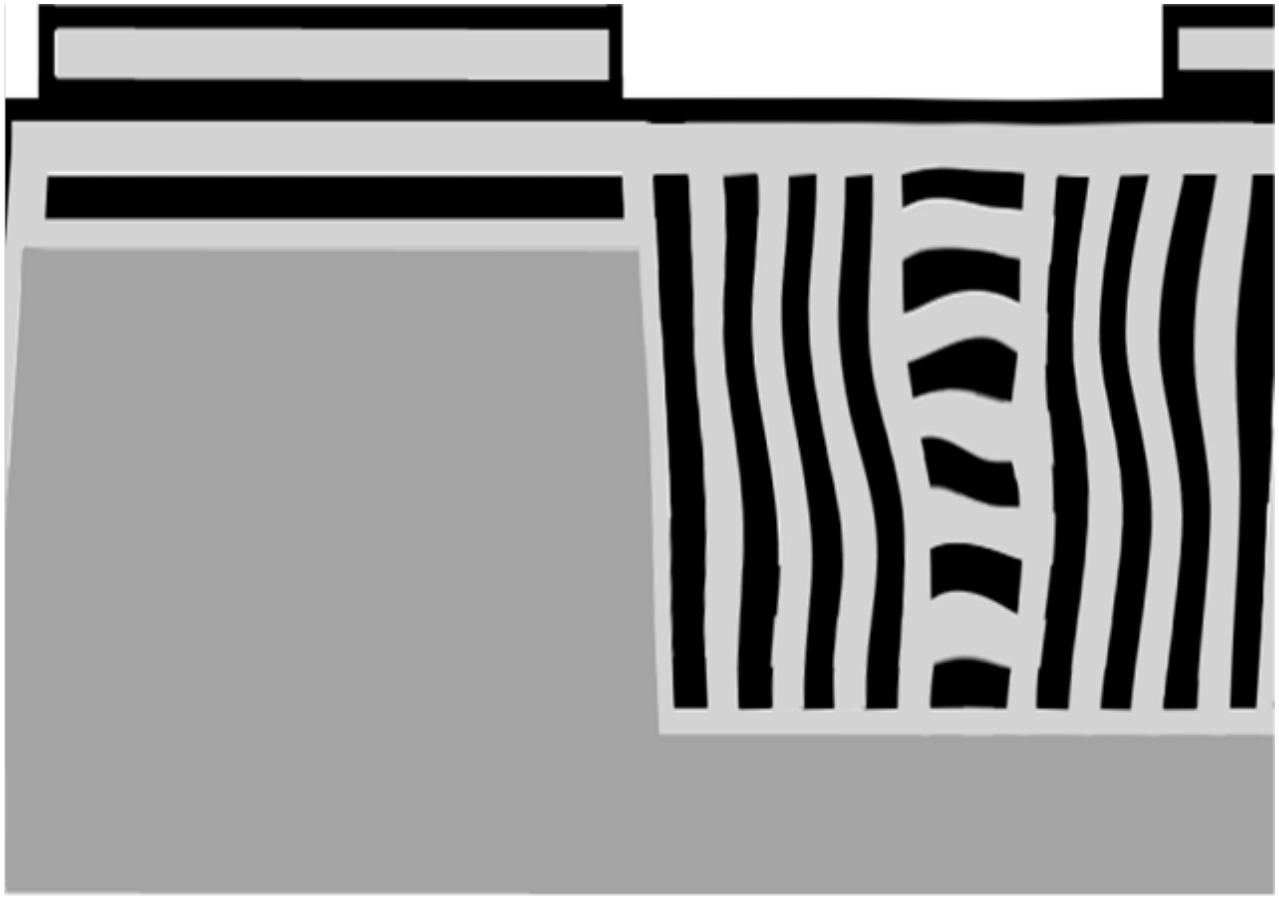

Fig 2. Diagram of expected orientation of lamellae, based on position with respect to the channels. Silicon substrate with etched channels is displayed in gray, with lighter and darker regions corresponding to the two polymer components of the lamellae.

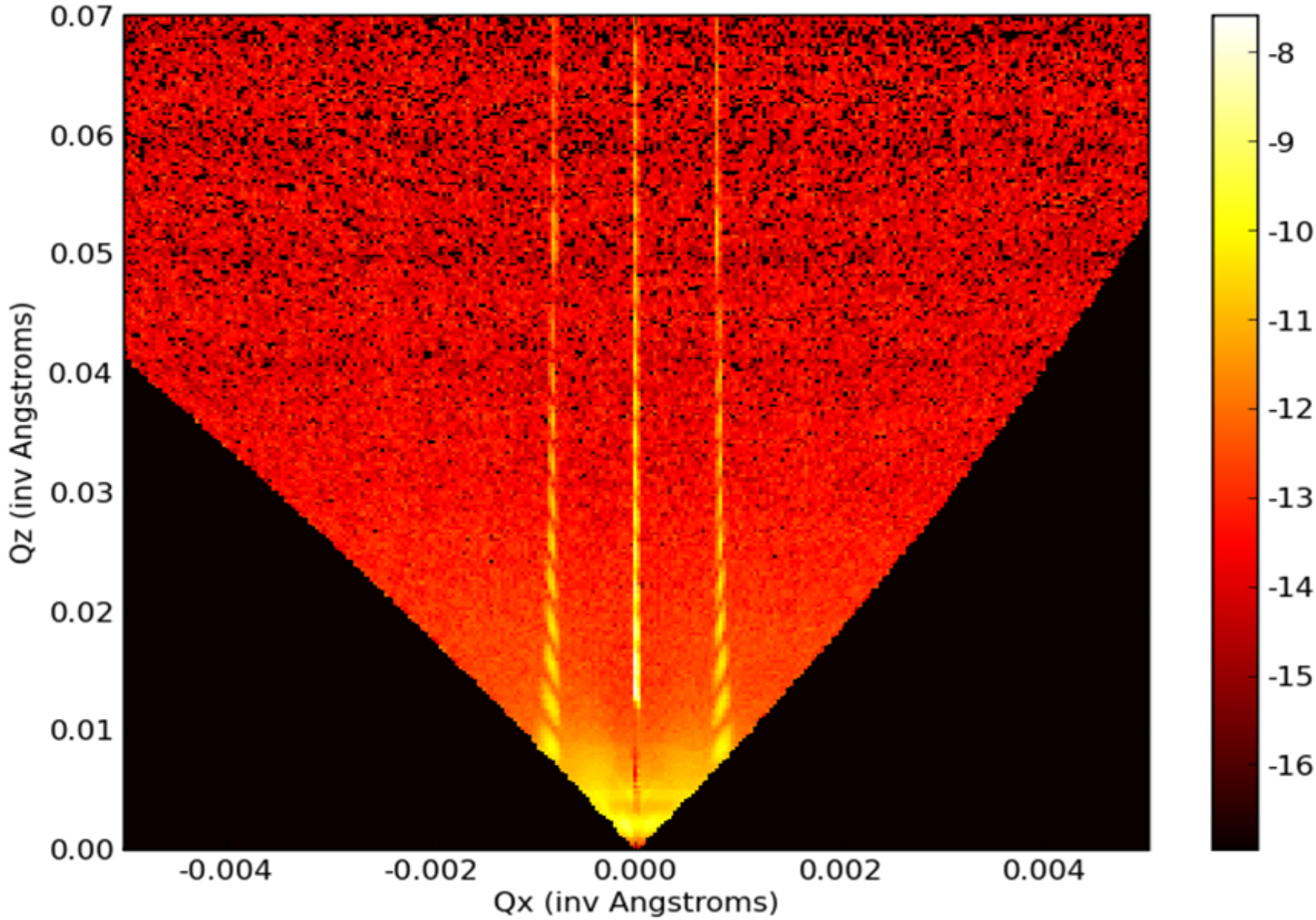

Neutron diffraction from silicon with channels but without polymer.

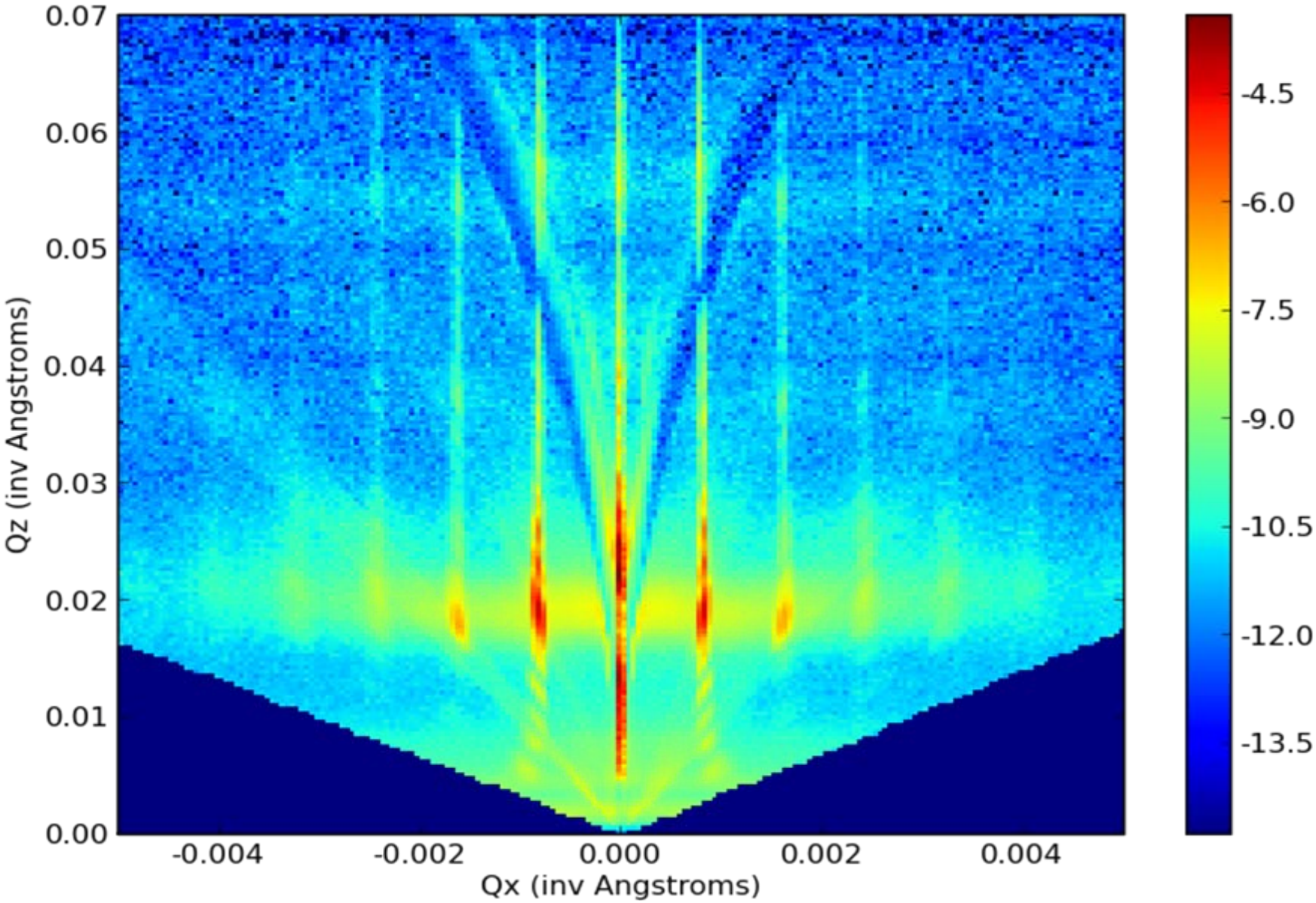

Neutron diffraction from Si channels filled with ordered diblock copolymer.

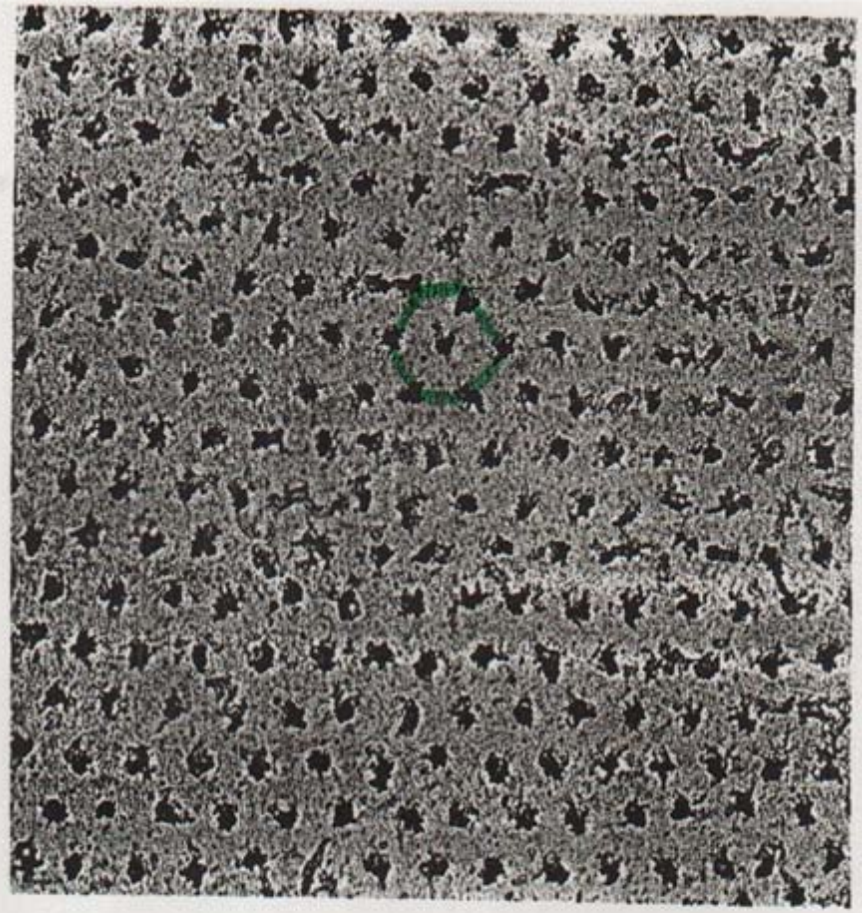

Figure 37 Triangular lattice of flux lines through top surface of a superconducting cylinder. The points of exit of the flux lines are decorated with fine ferromagnetic particles. The electron microscope image is at a magnification of 8300. (Courtesy of U. Essmann and H. Träuble.)

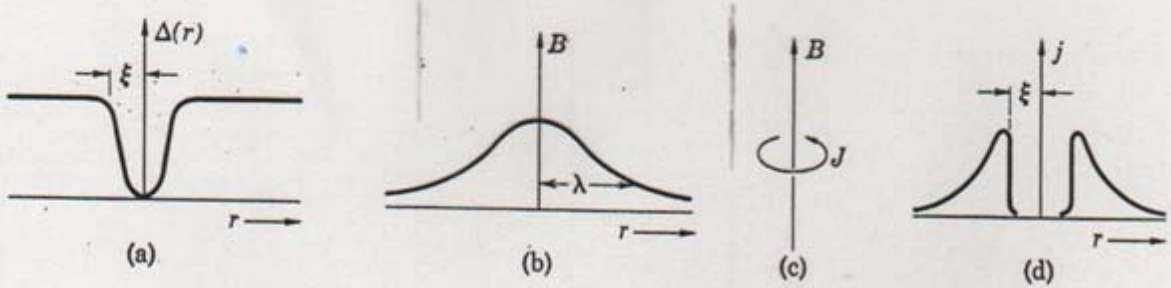

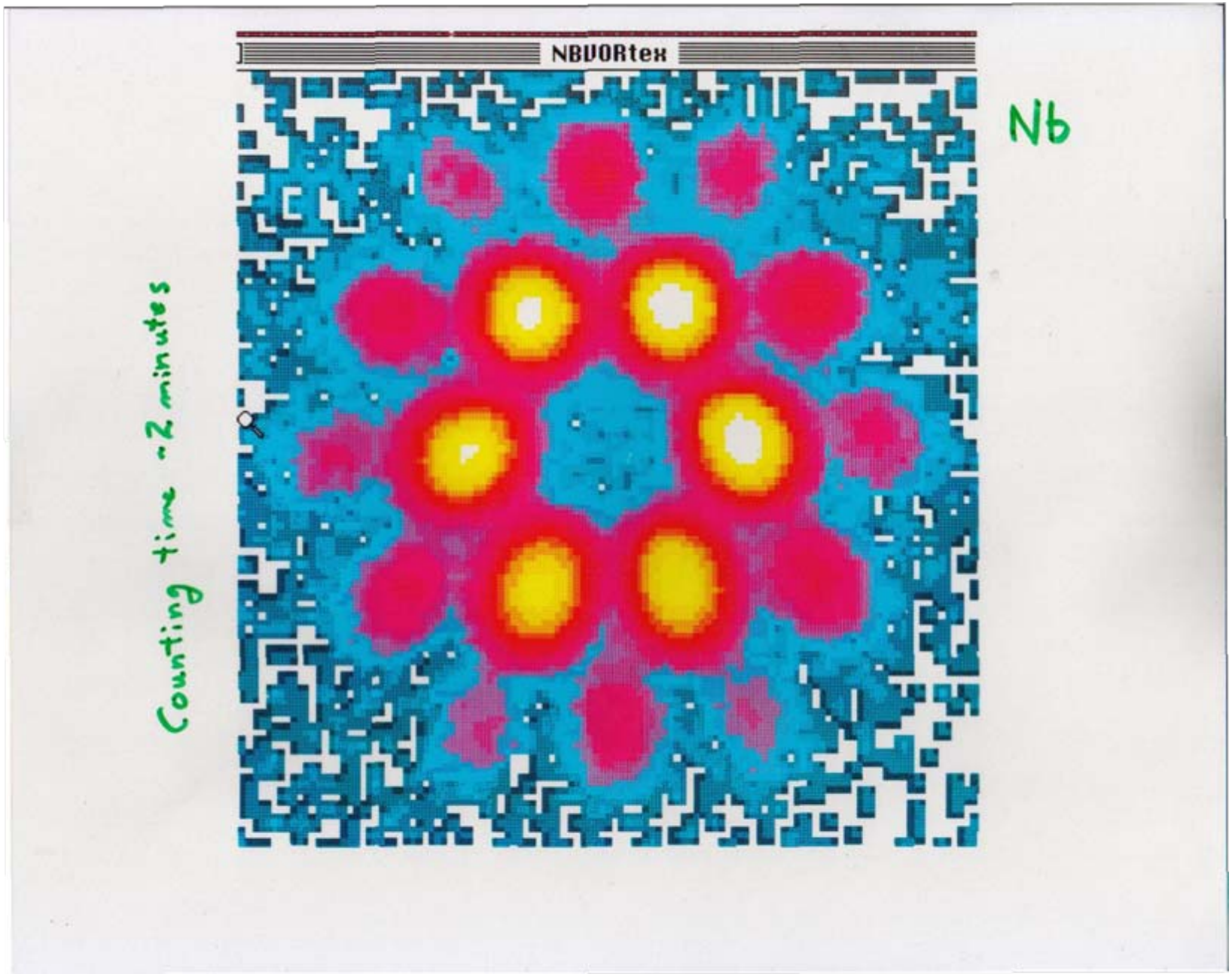

SANS diffraction pattern of vortex lattice in superconducting Nb – J.Lynn et al..

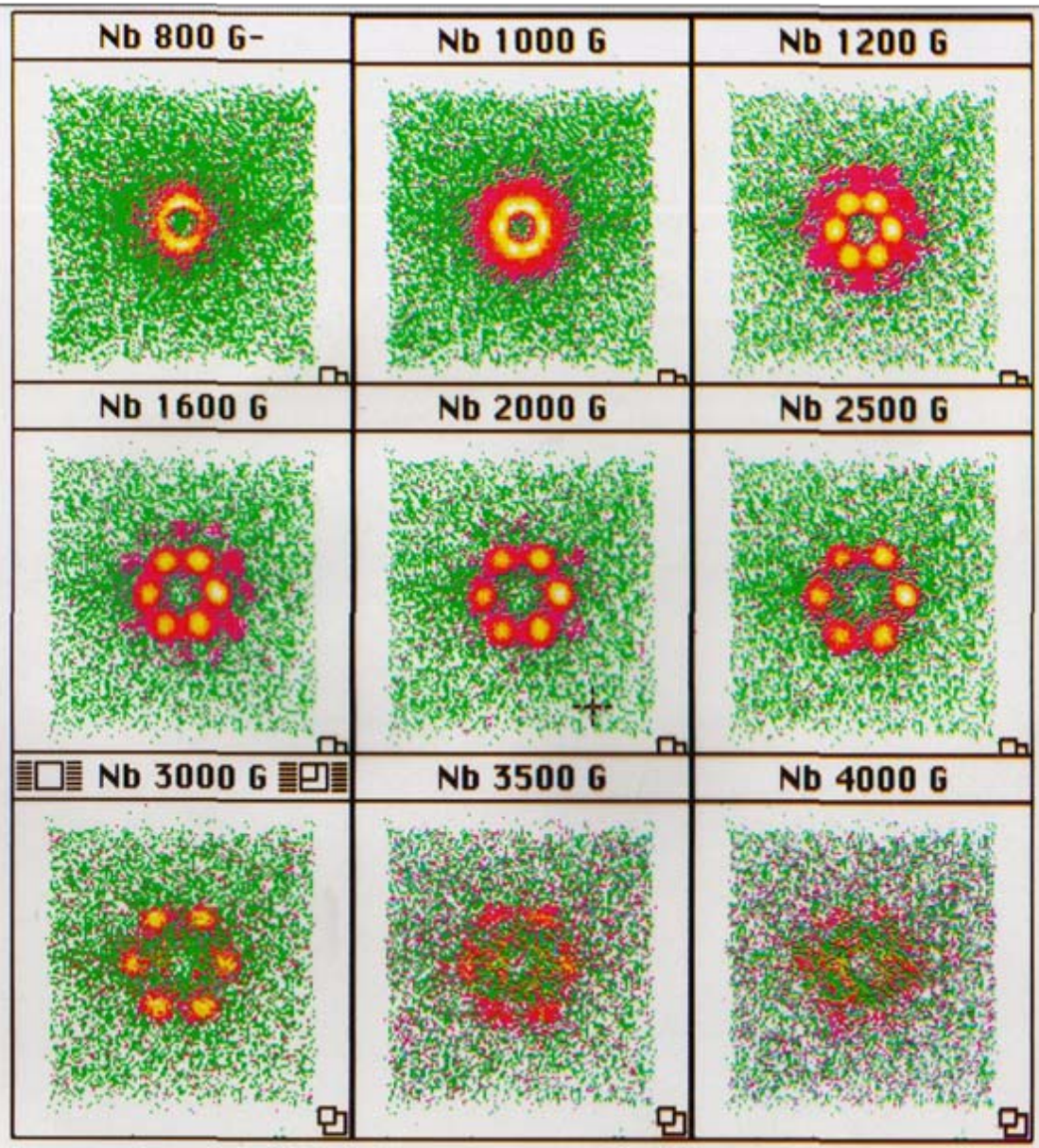

$T \approx 4.4\,K$

Vortex Lattice Dynamics in Niobium

J.W. Lynn, et al, Phys. Rev. Lett. 72, 3413 (1994)

$$\text{Reflectivity} = \frac{\text{Number of reflected neutrons}}{\text{Number of incident neutrons}} = |r|^2$$

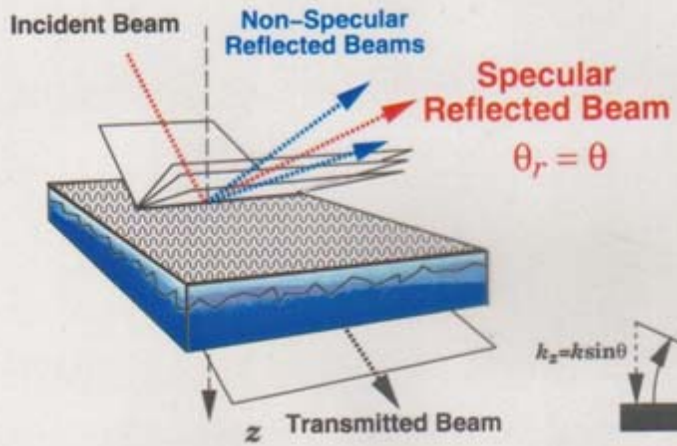

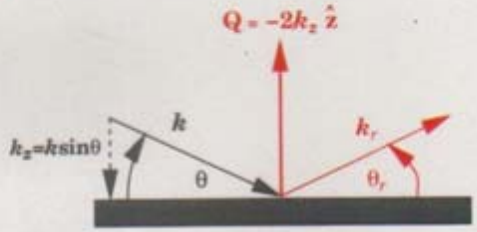

Specular reflection: $\overline{\rho}(z) = \langle\rho(x,y,z)\rangle_{xy}$

Non–Specular reflection: $\Delta\rho(x,y,z) = \rho(x,y,z) - \overline{\rho}(z)$

(AFTER N.F.BERK ET AL.)

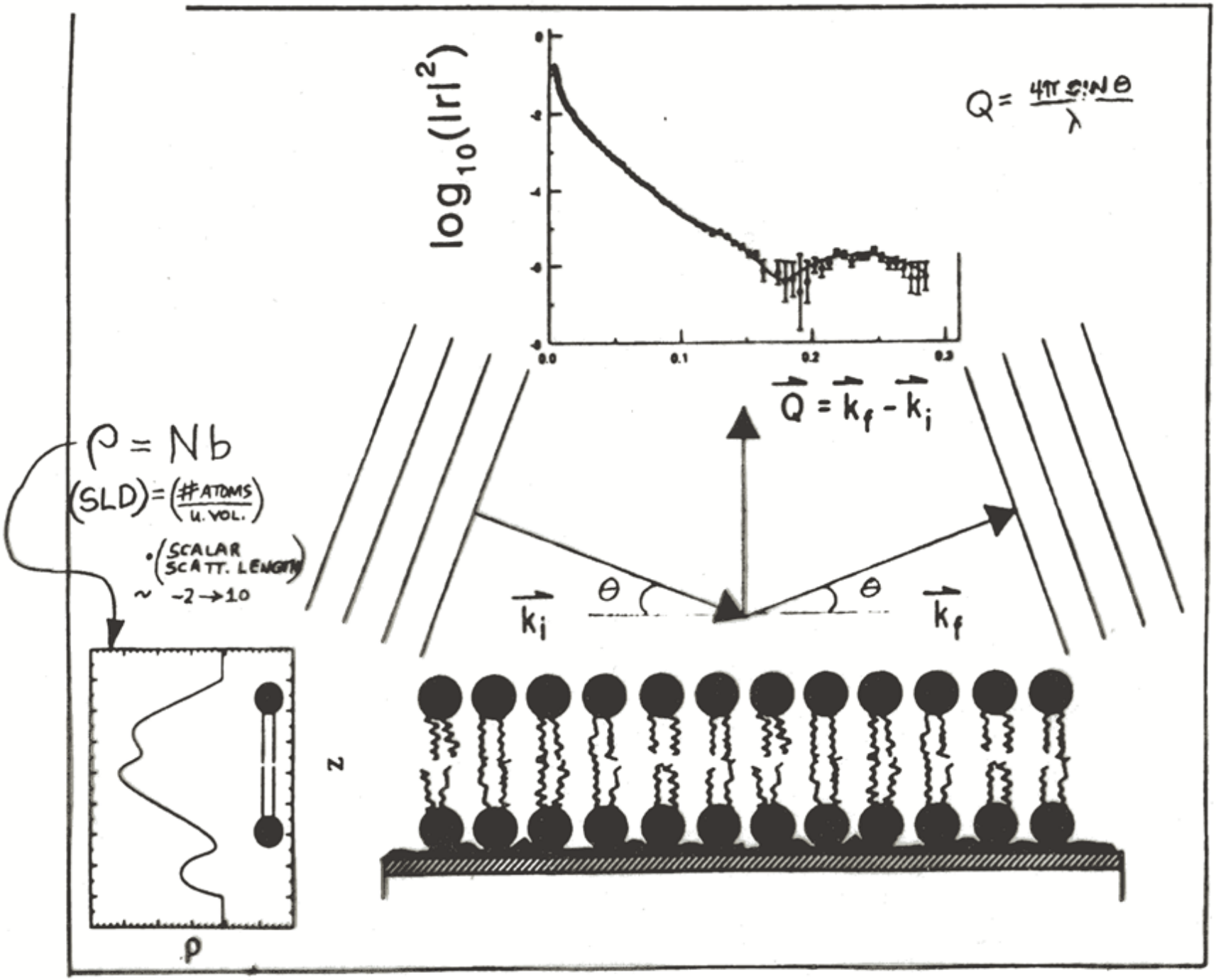
$\log_{10}(|r|^2)$
$Q = \frac{4\pi \sin\theta}{\lambda}$
$\vec{Q} = \vec{k}_f - \vec{k}_i$
$\rho = Nb$
(SLD) = (# ATOMS / U. VOL.) · (SCALAR SCATT. LENGTH)
~ −2 → 10
$\vec{k}_i$
θ
θ
$\vec{k}_f$
z
ρ

THE NEUTRON AS A PLANE WAVE PROPAGATING IN FREE SPACE

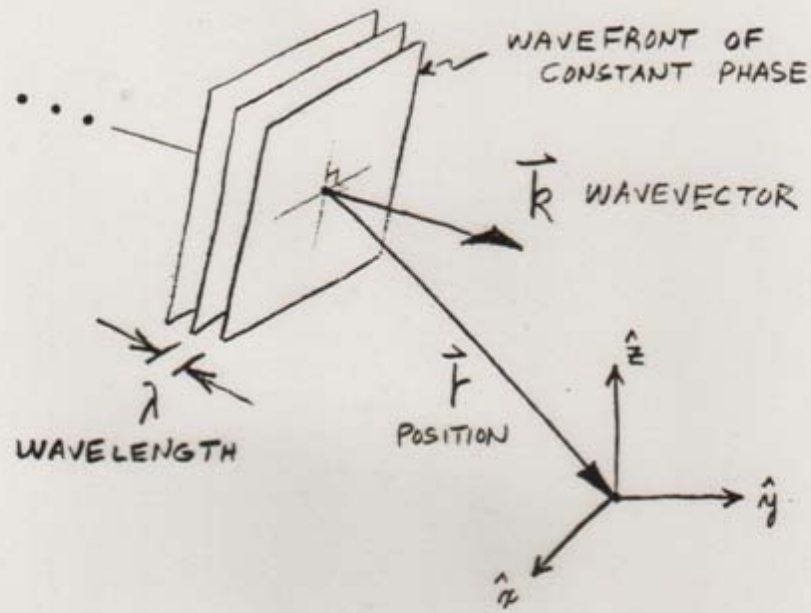

WAVEFUNCTION

$$\Psi \propto e^{i\vec{k}_0 \cdot \vec{r}}$$

$$\begin{cases} \vec{k}_0 = k_{0x}\hat{x} + k_{0y}\hat{y} + k_{0z}\hat{z} \\ \vec{r} = x\hat{x} + y\hat{y} + z\hat{z} \end{cases}$$

FOR $\vec{k}_0$ ALONG $\hat{z}$, FOR EXAMPLE,

$$\Psi \propto \cos\underbrace{(k_{0z} z)}_{=\left(\frac{2\pi}{\lambda} z\right)} + i \sin(k_{0z} z)$$

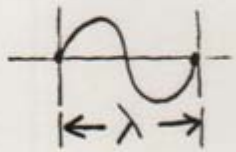

$|\Psi|^2 \propto$ PROBABILITY OF THE NEUTRON BEING THERE

FOR ELASTIC INTERACTIONS
TOTAL ENERGY OF THE
NEUTRON IS CONSTANT

TOTAL ENERGY = KINETIC ENERGY
+ POTENTIAL ENERGY

= CONSTANT

WAVE EQUATION OF MOTION
(SCHROEDINGER EQUATION)

$$\left[\underbrace{\frac{-\hbar^2}{2m}\nabla^2}_{K.E.} + \underbrace{V(\vec{r})}_{P.E.}\right]\Psi = \underbrace{E}_{T.E.}\Psi$$

$$\nabla^2 = \frac{\partial^2}{\partial x^2} + \frac{\partial^2}{\partial y^2} + \frac{\partial^2}{\partial z^2}$$

IN VACUUM

$$K.E._0 = \frac{\hbar^2 k_0^2}{2m}$$

IN THE CONTINUUM LIMIT

$$V(\vec{r}) = \frac{2\pi\hbar^2}{m} \sum_{j=1} N_j b_j = \frac{2\pi\hbar^2}{m}\rho$$

$(b = \mathrm{Re}\,b + i\,\mathrm{Im}\,b)$

NUMBER OF ATOMS OF TYPE j PER UNIT VOLUME

COHERENT SCATTERING "LENGTH" OF ATOM j

ρ = "SCATTERING LENGTH DENSITY" (SLD)

IN VACUUM:

$$E_0 = \frac{\hbar^2 k_0^2}{2m} + 0$$

IN A MATERIAL MEDIUM:

$$E = \frac{\hbar^2 k^2}{2m} + \frac{2\pi\hbar^2}{m}\rho$$

CONSERVATION OF ENERGY REQUIRES $E_0 = E$

$$\therefore \quad k^2 = k_0^2 - 4\pi\rho$$

THUS

$$\left[\nabla^2 + k^2\right]\Psi = 0$$

NOTE REFRACTIVE INDEX $n \equiv \frac{k}{k_0}$:

$$n^2 = 1 - \frac{4\pi\rho}{k_0^2}$$

REFLECTION FROM AN IDEAL FILM OR SLAB OF MATERIAL

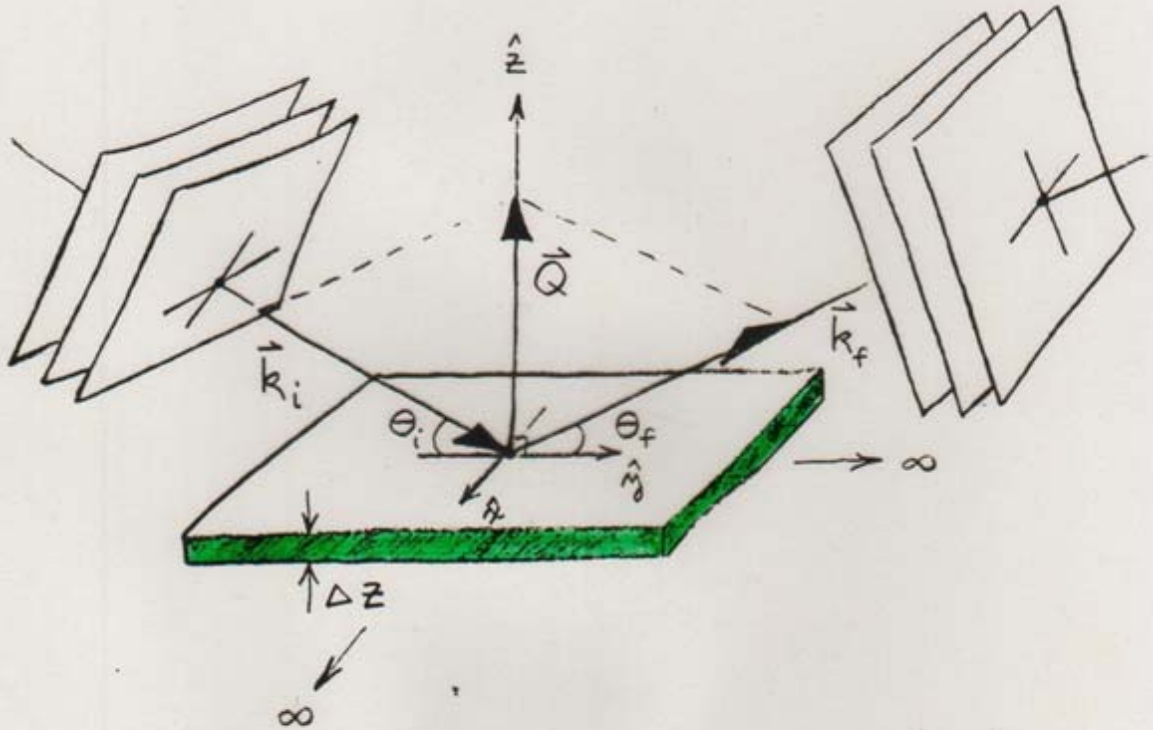

WAVEVECTOR TRANSFER $\vec{Q} = \vec{k}_f - \vec{k}_i$

$\rho = \rho(z)$ ONLY

EXPANDING $k^2 = k_0^2 - 4\pi\rho$,

$$k_x^2 + k_y^2 + k_z^2 + 4\pi\rho = k_{0x}^2 + k_{0y}^2 + k_{0z}^2.$$

NOW IF $\rho = \rho(z)$ ONLY, THEN

$\frac{\partial \rho}{\partial x}$ AND $\frac{\partial \rho}{\partial y}$, WHICH ARE

PROPORTIONAL TO THE GRADIENTS OF THE POTENTIAL OR FORCES IN THE RESPECTIVE DIRECTIONS, ARE EQUAL TO ZERO. THUS, NO FORCE ACTS ALONG THESE DIRECTIONS TO CHANGE k_x AND k_y. THEN

$k_x = k_{0x}$ AND $k_y = k_{0y}$ ARE

"CONSTANTS OF THE MOTION".

SUBSTITUTING $\Psi(\vec{r}) = e^{ik_{0x}x} e^{ik_{0y}y} \psi(z)$

INTO $[\nabla^2 + k^2]\Psi = 0$ GIVES

$$\left[\frac{\partial^2}{\partial z^2} + k_z^2\right]\psi(z) = 0$$

AND ∴ $k_z^2 = k_{0z}^2 - 4\pi\rho(z)$.

BECAUSE THERE IS NO CHANGE IN THE POTENTIAL IN THE X- OR Y- DIRECTIONS, THERE CAN BE NO MOMENTUM CHANGE IN THESE DIRECTIONS EITHER

THE IDEAL SLAB GEOMETRY WITH $\rho = \rho(z)$ ONLY GIVES RISE TO THE COHERENT "SPECULAR" REFLECTION OF A PLANE WAVE WHICH IS DESCRIBED BY A ONE-DIMENSIONAL WAVE EQUATION :

$$\left[\frac{\partial^2}{\partial z^2} + k_{0z}^2 - 4\pi\rho(z)\right]\psi(z) = 0$$

IN THIS CASE $\theta_i = \theta_f \equiv \theta$,

$|\vec{k}_i| = |\vec{k}_f|$ AND $Q = 2k\sin\theta$

$= 2k_z$

ALSO, $n_z^2 \equiv 1 - \frac{4\pi\rho(z)}{k_{0z}^2}$

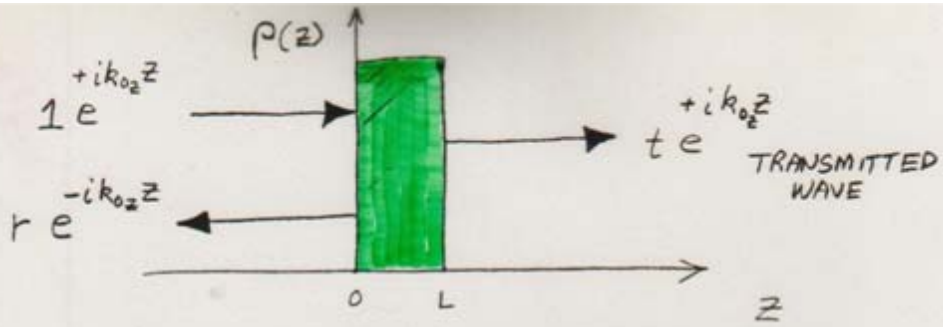

$$Q = 2k_{0z}$$

FROM THE WAVE EQUATION, IT IS POSSIBLE TO FIND A SOLUTION FOR THE REFLECTION AMPLITUDE IN INTEGRAL FORM (SEE ARTICLE PAGES):

$$r(Q) = \frac{4\pi}{iQ} \int_{-\infty}^{+\infty} \Psi(z)\, \rho(z)\, e^{+ik_{0z}z}\, dz$$

WHAT IS LOCALIZED AT z IN THE SLD PROFILE $\rho(z)$ IN "REAL" SPACE, IS DISTRIBUTED OVER THE REFLECTION AMPLITUDE $r(Q)$ IN THE RELATED SCATTERING OR "RECIPROCAL" SPACE

$$M_j = \begin{bmatrix} \cos\delta_j & \frac{1}{n_{x_j}}\sin\delta_j \\ -n_{x_j}\sin\delta_j & \cos\delta_j \end{bmatrix} \tag{11}$$

with $\delta_j = k_{ox}n_{xj}\Delta_j$, with n_{sx} and n_{ox} corresponding to the substrate and incident medium, respectively. The jth matrix M_j corresponds to the jth slab of thickness Δ_j wherein the scattering density is assumed to be constant and equal to ρ_j. The amplitude of the incident wave is assumed to be unity. The transmission and reflectivity are $T^*T = |T|^2$ and $R^*R = |R|^2$, respectively, and can be obtained directly from Equation (9).

Thus, for a given model potential, it is straightforward to calculate the expected reflectivity. Unfortunately, the converse of this statement is not necessarily true, as will be discussed in more detail in Section 4.

At this point it is useful to consider an alternate derivation of the reflectivity from which the Born approximation (corresponding to the kinematic limit which is discussed below) and other useful results can be directly obtained. Suppose that there exist two arbitrary but different density profiles $\rho_1(x)$ and $\rho_2(x)$ for which the corresponding, separate reflectivities are to be calculated. In each case we take the incident wave to propagate from left to right. We then have to solve the following pair of equations (derived from equations 6 and 7):

$$\psi_j''(x) + [k_{o_x}^2 - 4\pi\rho_j(x)]\,\psi_j(x) = 0 \qquad j = 1,2 \tag{12}$$

for $-\infty < x < \infty$ where $\psi_1(x)$ and $\psi_2(x)$ are the exact solutions in each case. From these we can construct the Wronskian function

$$W(x) \equiv W[\psi_1(x), \psi_2(x)] = \psi_1(x)\psi_2'(x) - \psi_1'(x)\psi_2(x). \tag{13}$$

Differentiating both sides of eq. (13) and using eq. (12) we obtain

$$W'(x) = -\psi_1(x)4\pi\rho_{12}(x)\psi_2(x) \tag{14}$$

where

$$\rho_{12}(x) \equiv \rho_1(x) - \rho_2(x) \quad . \tag{15}$$

Equation (14) tells us that W(x) is a constant over intervals where the two density profiles coincide, $\rho_1(x) = \rho_2(x)$, which is a property we will exploit to obtain a formula relating the reflectivities for each profile. First, assume that $\rho_1 \neq \rho_2(x)$ only within an interval $\ell_1 < x < \ell_2$. We allow subintervals of (ℓ_1, ℓ_2) where $\rho_1(x) = \rho_2(x)$, but we demand finite ℓ_1 and ℓ_2 such that $\rho_1(x) = \rho_2(x)$ for all $x < \ell_1$ and for all $x > \ell_2$. We also assume that the wave is incident in vacuum so for $x < \ell_1$, $\rho_1(x) = \rho_2(x) = 0$. The wavefunctions for $x < \ell_1$ are then

$$\psi_j(x) = e^{ik_{o_x}x} + R_j e^{-ik_{o_x}x} \tag{16}$$

where R_1 and R_2 are the reflection amplitudes for each problem. Similarly, we assume that each density profile has a common substrate so that for $x > \ell_2$, $\rho_1(x) = \rho_2(x) = \rho(\infty)$. The wavefunctions for $x > \ell_2$ are then

$$\psi_j(x) = T_j\, e^{iKx} \tag{17}$$

where

$$K = \sqrt{k_{o_x}^2 - 4\pi\rho(\infty)} \tag{18}$$

and T_1 and T_2 are the transmission amplitudes in each problem. Now we see that for the given pair of profile functions $\rho_1(x)$ and $\rho_2(x)$, W(x) is uniquely determined everywhere and varies with x only in (ℓ_1, ℓ_2), where $\rho_1(x)$ and $\rho_2(x)$ can differ. Substituting (17) into (13) we obtain

$$W(x) = 0 \tag{19}$$

for all $x \geq \ell_2$, since $\psi_1(x)$ and $\psi_2(x)$ are proportional to one another (linearly dependent) in this region. However, substituting (16) into (13) we get

$$W(x) = 2ik_{o_x}(R_1 - R_2) \tag{20}$$

for all $x \leq \ell_1$, which is a complex constant. Finally, for $\ell_1 < x < \ell_2$ we integrate both sides of equation (14) to obtain

$$\int_{\ell_1}^{\ell_2} W'(x)dx = W(\ell_2) - W(\ell_1) = -\alpha_{12} \tag{21}$$

where

$$\alpha_{12} = \int_{\ell_1}^{\ell_2} \psi_1(x)4\pi\rho_{12}(x)\psi_2(x)dx \quad . \tag{22}$$

Now W(x) is continuous everywhere since $\psi_j(x)$ and $\psi_j'(x)$ are. Thus, evaluating (19) and (20) at $x = \ell_2$ and $x = \ell_1$, respectively, we find $W(\ell_2) = 0$ and $W(\ell_1) = 2ik_{ox}(R_1 - R_2)$. Thus, from equation (21) we get

$$R_1 = R_2 + \frac{\alpha_{12}}{iQ} \tag{23}$$

where again $Q = 2k_{ox}$ is the wavevector transfer. Equation (23) is the general formula we set out to derive and is a handy starting point for exact treatments as well as approximation schemes.

For example, consider any $\rho(x)$ which vanishes identically for $x < \ell_1$ and for $x > \ell_2$. Then, in equation (23) we can set $\rho_1(x) = \rho(x)$, $\psi_1(x) = \psi(x)$, and $R_1 = R$ whereas for the "other" density profile we take $\rho_2(x) = 0$ everywhere so that $\psi_2(x) = \exp(ik_{ox}x)$ and $R_2 = 0$. Combining equations (22) and (23) then gives the exact solution of the reflectivity for an arbitrary scattering density profile $\rho(x)$:

$$R = \frac{4\pi}{iQ}\int_{-\infty}^{+\infty} \psi(x)\rho(x)e^{ik_{o_x}x}dx \tag{24}$$

where we have formally extended the integration over all x, though only the region where $\rho(x) \neq 0$ contributes. Although it may not be obvious from the derivation, equation (24) also holds if we allow $\rho(x)$ to be nonzero as $x \to \infty$, as long as the integral exists. Note that (24) requires, to be exact, the exact wavefunction $\psi(x)$ wherever $\rho(x) \neq 0$. The corresponding expression for the reflectivity $|R|^2$, is

$\psi(z)$ INSIDE THE MEDIUM IS GENERALLY UNKNOWN:

BORN APPROXIMATION REPLACES $\psi(z)$ WITH THE INCIDENT WAVE FUNCTION $e^{+ik_{0z}z}$ BASED ON THE ASSUMPTION THAT $\psi(z)$ IS NOT SIGNIFICANTLY DISTORTED FROM THE FREE SPACE FORM (WEAK INTERACTION): THEN

FOURIER TRANSFORM

$$r(Q) \simeq \frac{4\pi}{iQ} \int_{-\infty}^{+\infty} \rho(z)\, e^{iQz}\, dz$$

FOR A REAL POTENTIAL $\rho(z)$

$$\mathrm{Re}\, r(Q) \simeq \frac{4\pi}{Q} \int_{-\infty}^{+\infty} \rho(z) \sin(Qz)\, dz$$

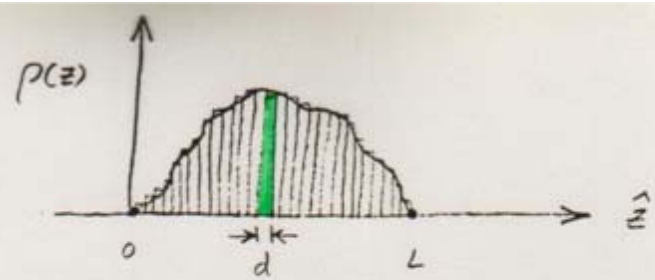

ARBITRARY POTENTIAL DIVIDED INTO RECTANGULAR SLABS OF WIDTH d AND CONSTANT ρ

THEN

(BORN APPROX.)

$$\mathrm{Re}\, r(Q) \simeq \frac{4\pi}{Q} \int_0^L \rho(z) \sin(Qz)\, dz$$

BECOMES

$$\mathrm{Re}\, r(Q_j) \simeq \frac{4\pi}{Q_j} \sum_{\ell=1}^{N} \int_{(\ell-1)d}^{\ell d} \rho_\ell \sin(Q_j z)\, dz$$

$$= \frac{-4\pi}{Q_j^2} \sum_{\ell=1}^{N} \rho_\ell \left[\cos(Q_j z)\right]_{(\ell-1)d}^{\ell d}$$

SET OF Re r FOR DIFFERENT VALUES OF Q OR θ

$$\left\{ \begin{aligned} \mathrm{Re}\, r_1 &= \mathcal{C}_{11} \rho_1 + \mathcal{C}_{12} \rho_2 + \cdots + \mathcal{C}_{1N} \rho_N \\ \mathrm{Re}\, r_2 &= \mathcal{C}_{21} \rho_1 + \mathcal{C}_{22} \rho_2 + \cdots + \mathcal{C}_{2N} \rho_N \\ &\vdots \\ \mathrm{Re}\, r_N &= \mathcal{C}_{N1} \rho_1 + \mathcal{C}_{N2} \rho_2 + \cdots + \mathcal{C}_{NN} \rho_N \end{aligned} \right.$$

SOLVE SIMULTANEOUS EQUATIONS FOR ρ's GIVEN Re r's

e.g., SVD, EIGENVALUE PROBLEM FORMULATION, ...

$$\underbrace{\mathrm{Re}\; r_{BA}(Q)\left[\frac{Q^2}{8\pi \sin\left(\frac{Qd}{2}\right)}\right]}_{\equiv\, \mathcal{F}(Q)} = \sum_{j=1}^{N} \rho_j \sin\left[\frac{(2j-1)Qd}{2}\right]$$

$$\int_0^{\pi} \sin m\theta \sin n\theta \, d\theta = \begin{cases} 0 & m,n \text{ INTEGERS}, \; m \neq n \\ \frac{\pi}{2} & m,n \text{ INTEGERS}, \; m = n \end{cases}$$

ORTHOGONALITY

$$\rho_j = \frac{d}{4\pi^2} \int_0^{\frac{\pi}{d}} Q^2 \,\mathrm{Re}\; r_{BA}(Q) \frac{\sin\left[\frac{(2j-1)Qd}{2}\right]}{\sin\left(\frac{Qd}{2}\right)} \, dQ$$

$2\theta = 180^\circ$

$$\left(= \frac{4\pi}{\lambda} \sin(90^\circ)\right)$$

$\lambda(\mathring{A})$	Q_{MAX} $(\mathring{A}^{-1})$	$D_{MIN}(\mathring{A}) = \frac{2\pi}{Q_{MAX}} = \frac{\lambda}{2}$
5	2.513	2.5
10	1.256	5
50	0.251	25
100	0.125	50
500	0.025	250
1000	0.012	500
5000	0.002	2500

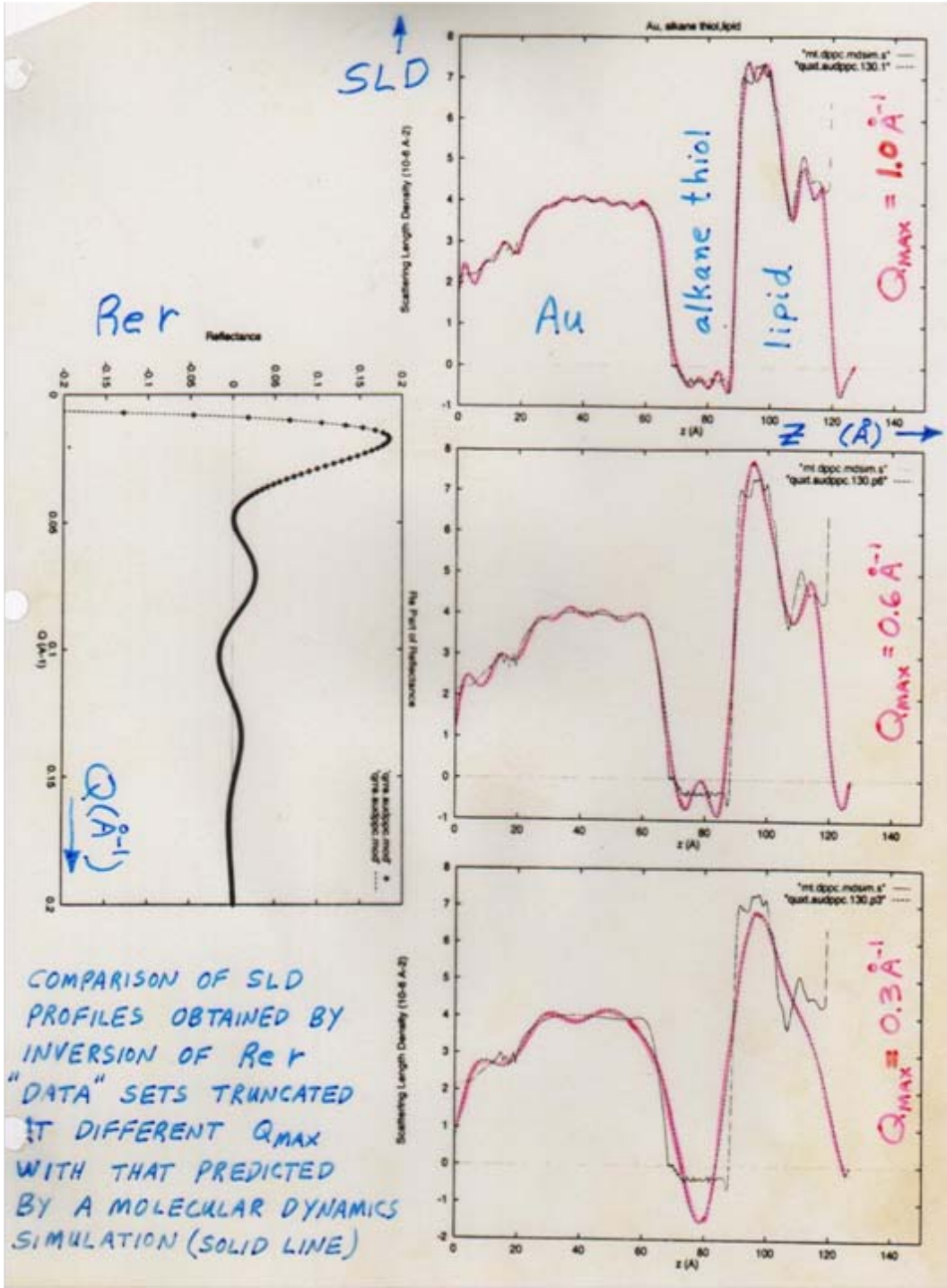

COMPARISON OF SLD PROFILES OBTAINED BY INVERSION OF Re r "DATA" SETS TRUNCATED AT DIFFERENT Q_{MAX} WITH THAT PREDICTED BY A MOLECULAR DYNAMICS SIMULATION (SOLID LINE)

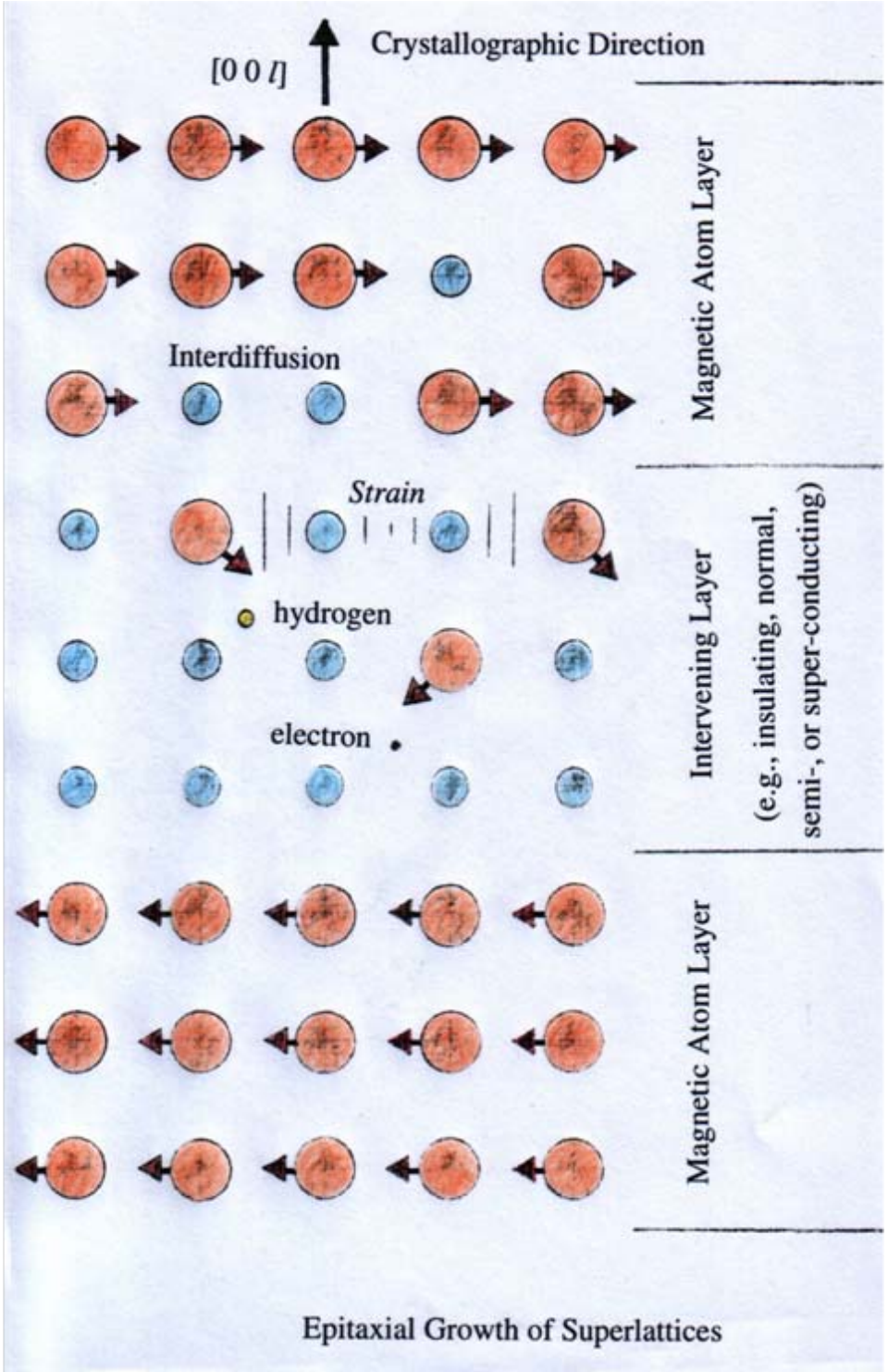

Epitaxial Growth of Superlattices

"REFLECTIVITY" REGIME

CRYSTAL "DIFFRACTION" REGIME

LOW Q : HIGHER SENSITIVITY FOR COMPOSITION PROFILE

HIGH Q : HIGHER SENSITIVITY FOR STRAIN OR LATTICE SPACING PROFILE

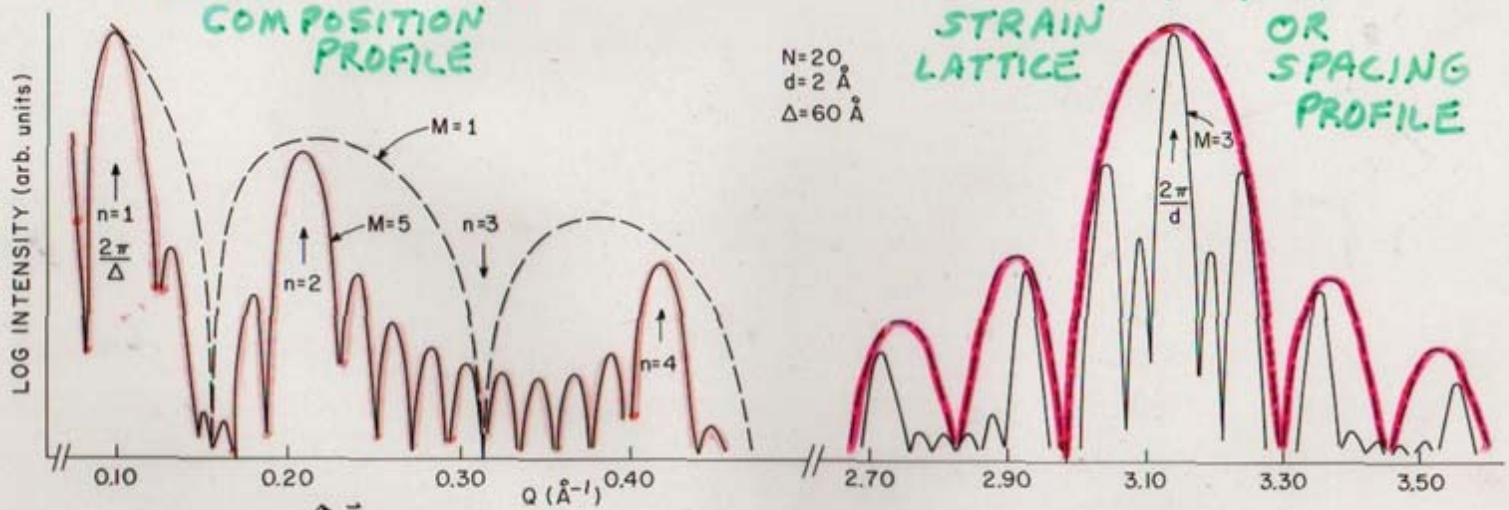

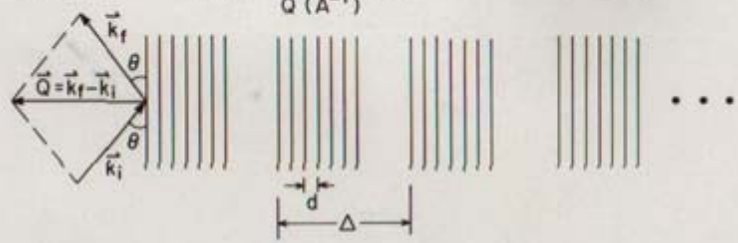

$$|R|^2_{KIN} = \left(\frac{4\pi}{Q}\right)^2 \left| \sum_{m=1}^{M} \sum_{n=1}^{N} \rho e^{iQ(nd+m\Delta)} \right|^2$$

$$= \left(\frac{4\pi}{Q}\right)^2 \rho^2 \left| \frac{\sin(NQd/2)}{\sin(Qd/2)} \right|^2 \left| \frac{\sin(MQ\Delta/2)}{\sin(Q\Delta/2)} \right|^2$$

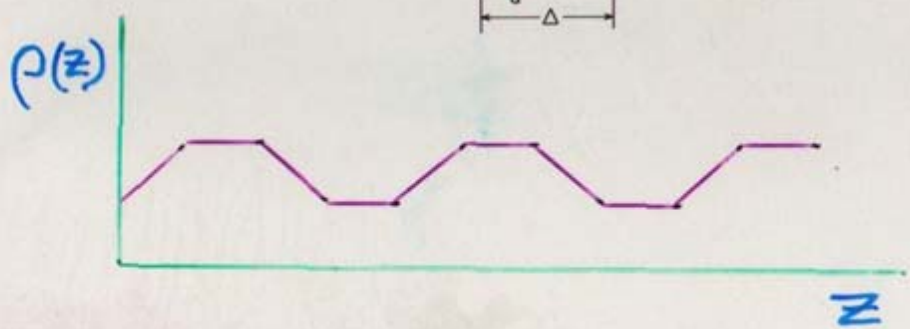

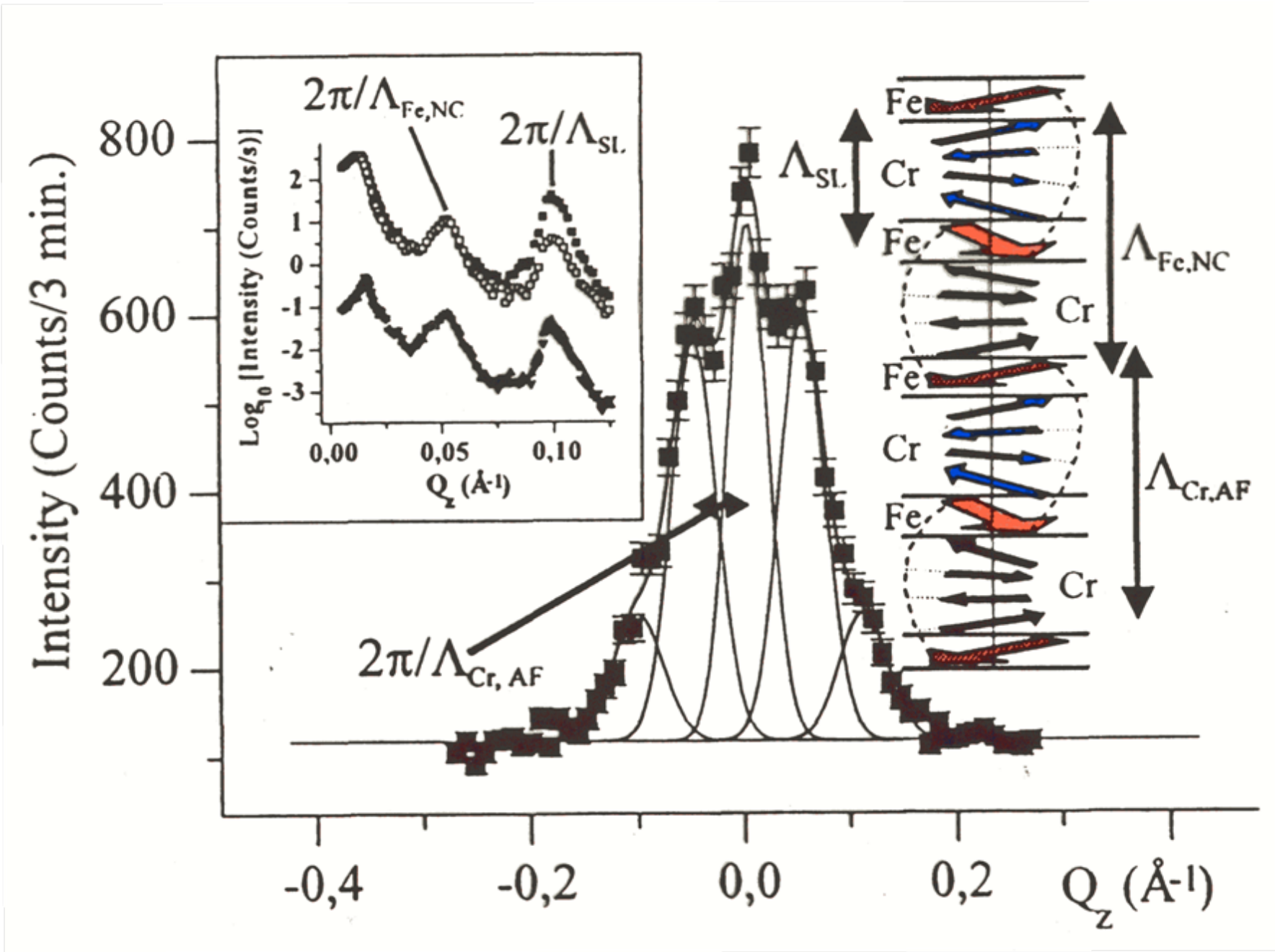

(Andreas Schreyer et al. - polarized neutron reflection/diffraction)

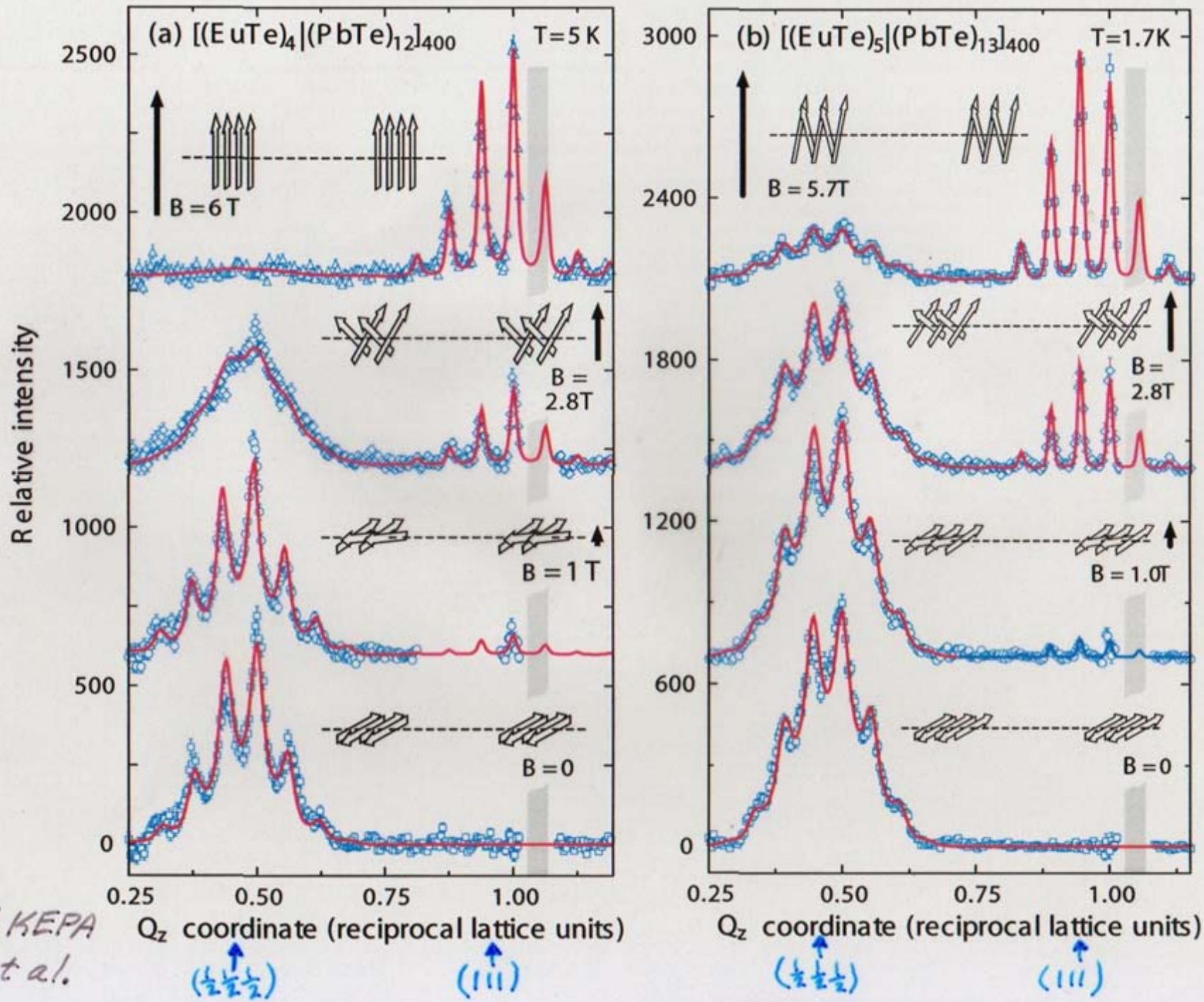
(a) [(EuTe)4|(PbTe)12]400
T=5 K
B = 6 T
B = 2.8T
B = 1 T
B = 0
Relative intensity
2500
2000
1500
1000
500
0
0.25
0.50
0.75
1.00
Qz coordinate (reciprocal lattice units)
(b) [(EuTe)5|(PbTe)13]400
T=1.7K
B = 5.7T
B = 2.8T
B = 1.0T
B = 0
3000
2400
1800
1200
600
0
0.25
0.50
0.75
1.00
Qz coordinate (reciprocal lattice units)

H. KEPA et al.

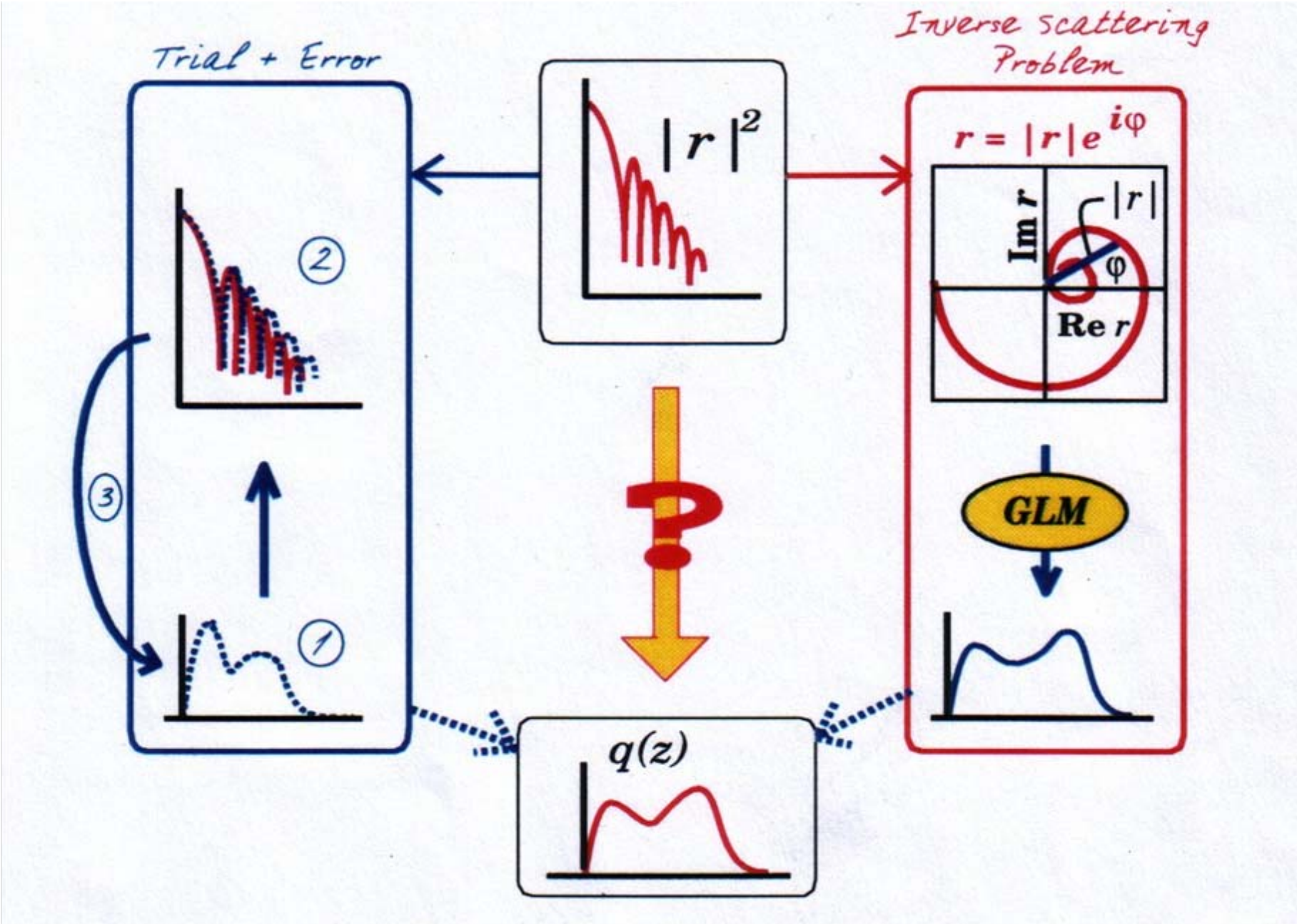

(Figure after Norm Berk et al.)

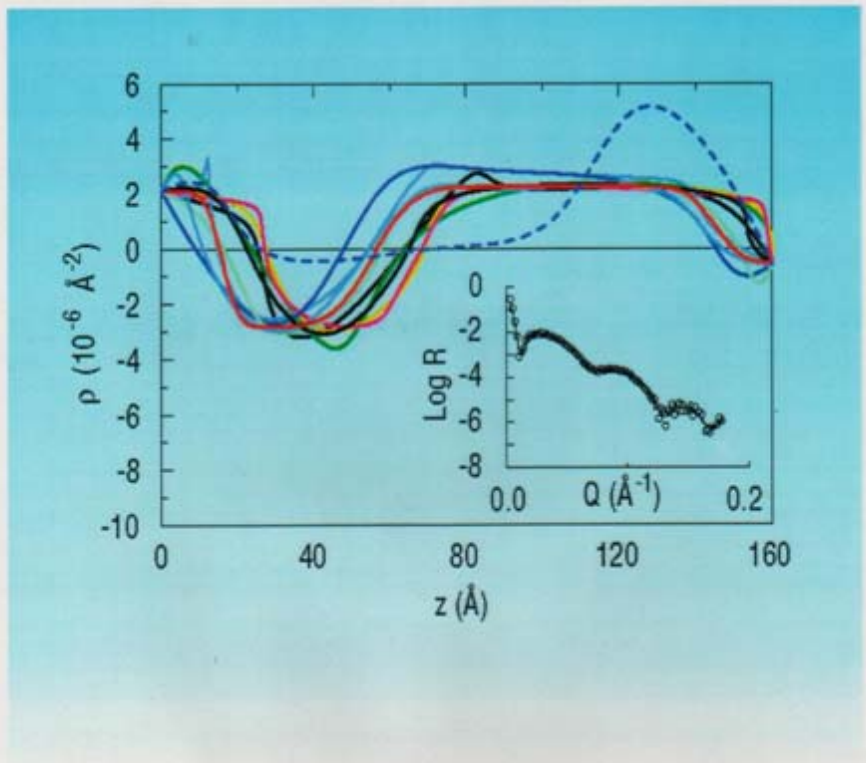

FIGURE 1. Family of scattering length density profiles obtained by model-independent fitting of the reflectivity data in the inset. The profile represented by the blue dashed line is unphysical for this Ti/TiO film system yet generates a reflectivity curve that fits the data with essentially equivalent goodness-of-fit (all the reflectivity curves corresponding to the SLD's shown are plotted in the inset but are practically indistinguishable from one another).

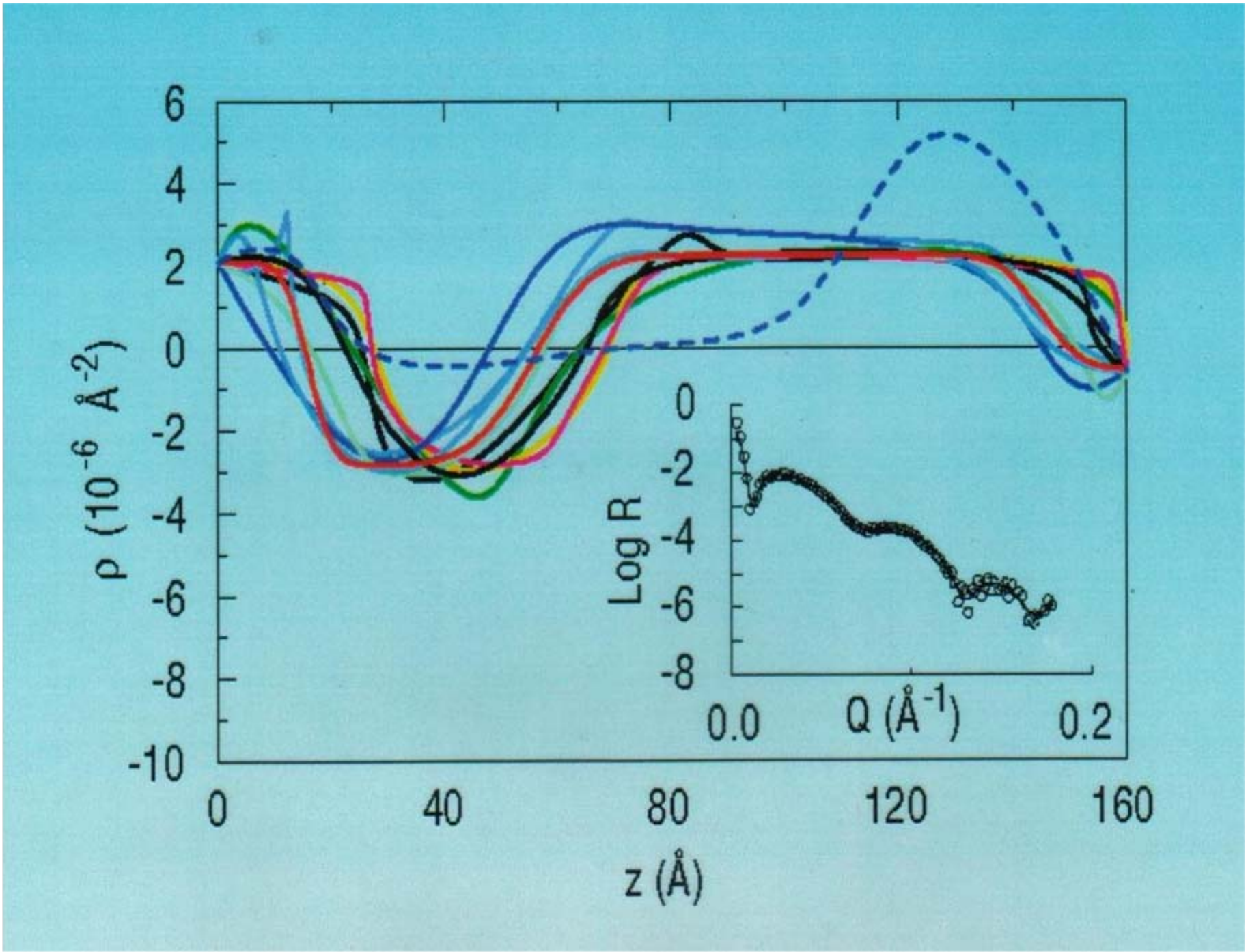
6
4
2
0
-2
-4
-6
-8
-10
ρ (10^-6 Å^-2)
0
40
80
120
160
z (Å)
0
-2
-4
-6
-8
Log R
0.0
Q (Å^-1)
0.2

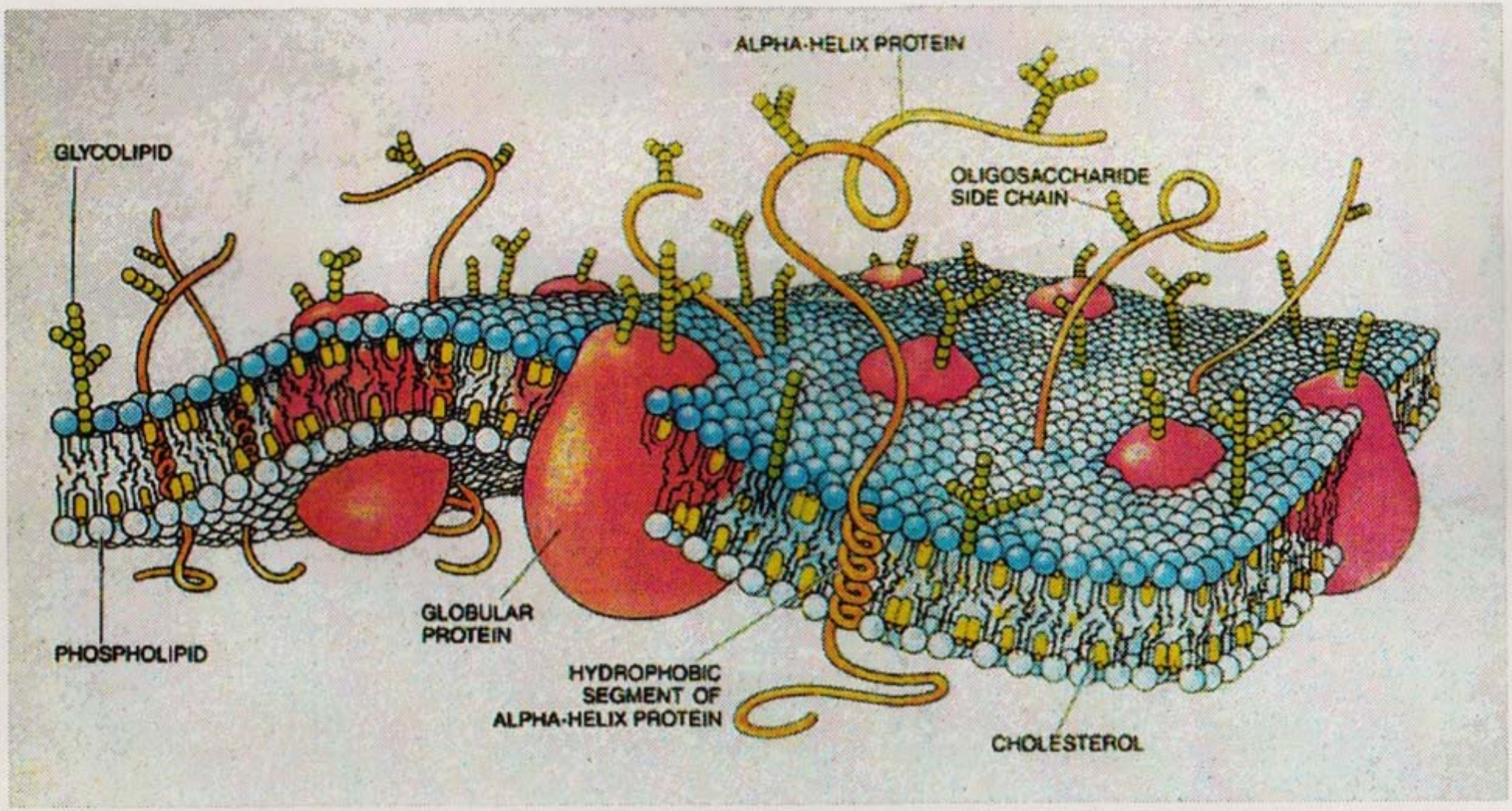

BORROWED FROM SCIENTIFIC AMERICAN

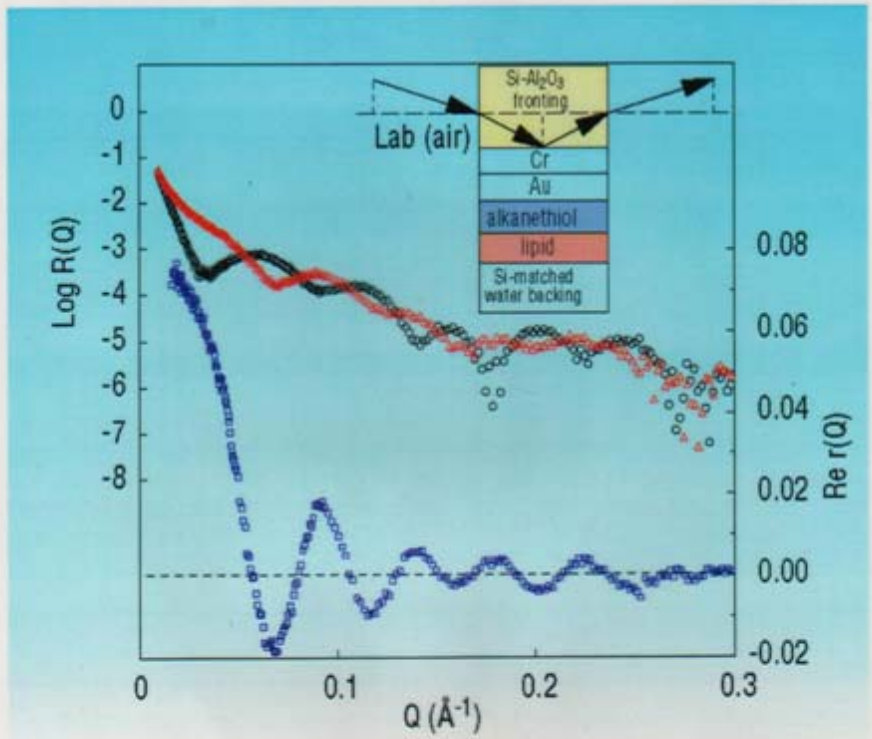

FIGURE 2. Reflectivity curves for the thin film system depicted schematically in the inset, one for a Si fronting (red triangles), the other for Al_2O_3 (black circles). The curve in the lower part of the figure (blue squares) is the real part of the complex reflection amplitude for the films obtained from the reflectivity curves by the method described in the text.

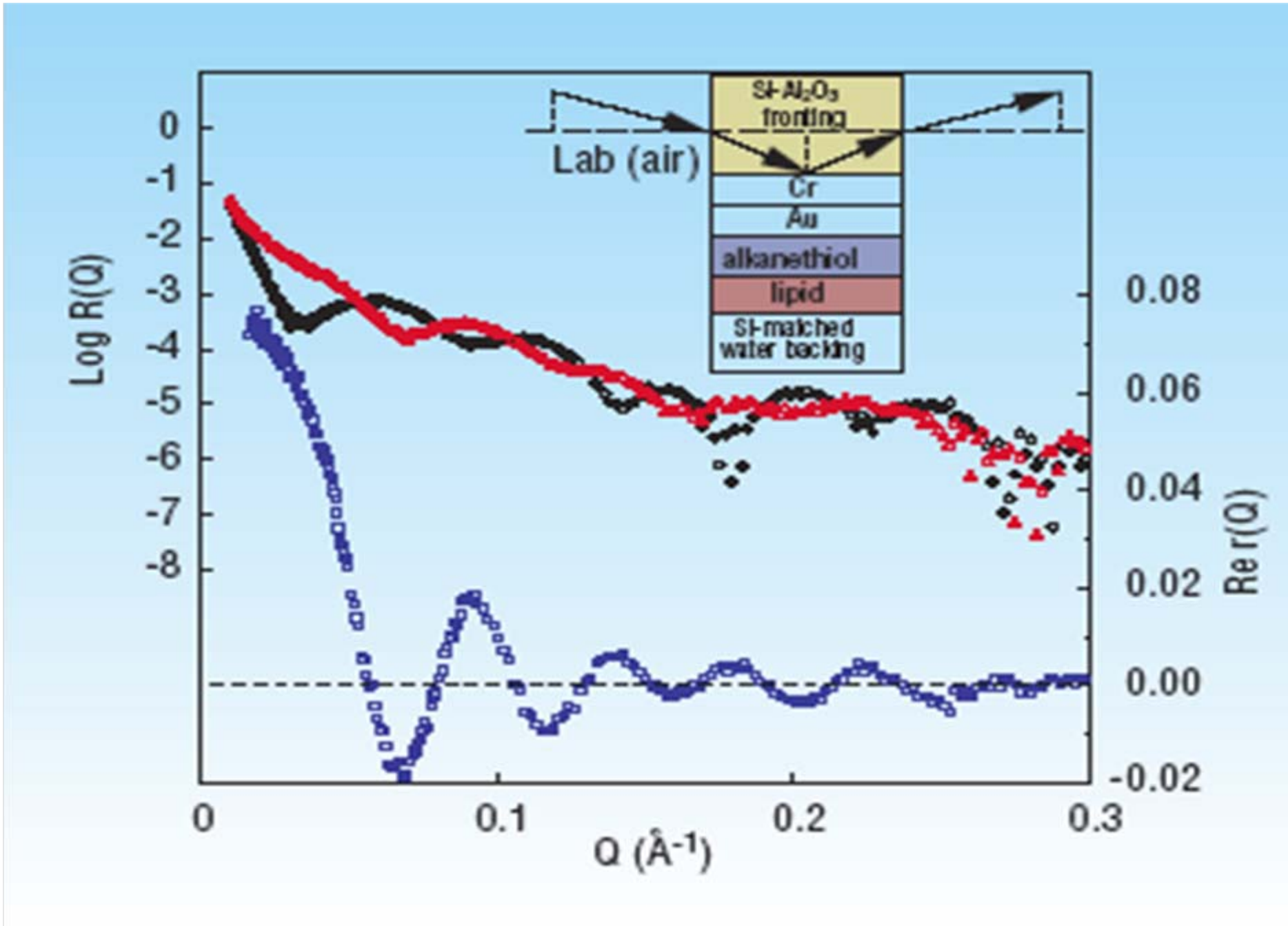
Si-Al2O3 fronting
Lab (air)
Cr
Au
alkanethiol
lipid
Si-matched water backing
Log R(Q)
Re r(Q)
Q (Å-1)
0
-1
-2
-3
-4
-5
-6
-7
-8
0.08
0.06
0.04
0.02
0.00
-0.02
0
0.1
0.2
0.3

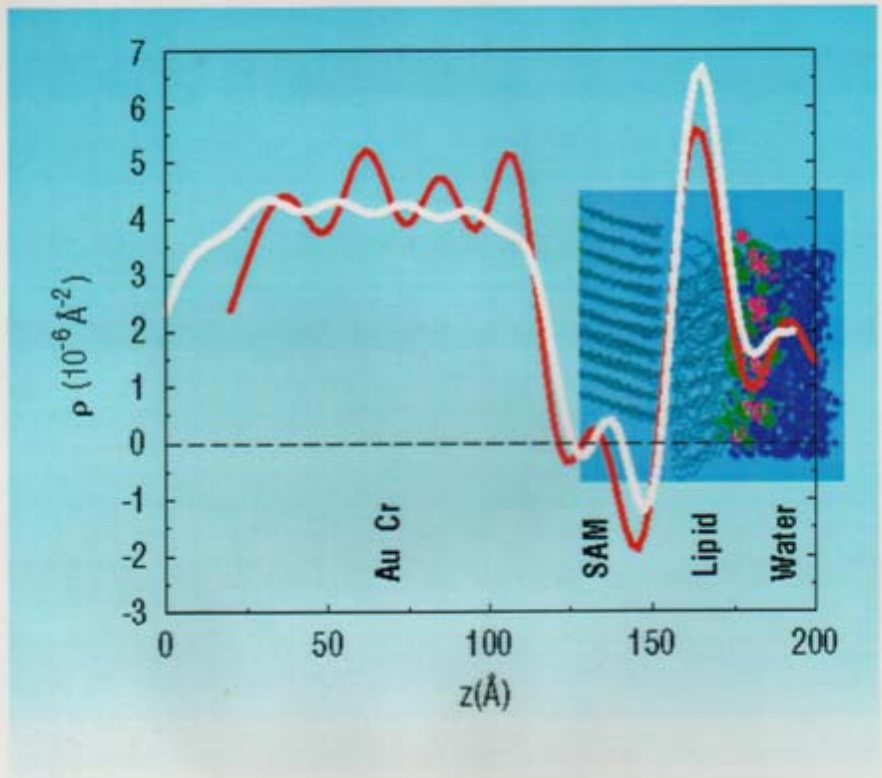

FIGURE 3. SLD profile (red line) resulting from a direct inversion of the Re r of Fig. 2 compared with that predicted by a molecular dynamics simulation (white line) as discussed in the text. The headgroup for the Self-Assembled-Monolayer (SAM) at the Au surface in the actual experiment was ethylene oxide and was not included in the simulation but, rather, modelled separately as part of the Au. Also, the Cr-Au layer used in the model happened to be 20 Å thicker than that actually measured in the experiment.

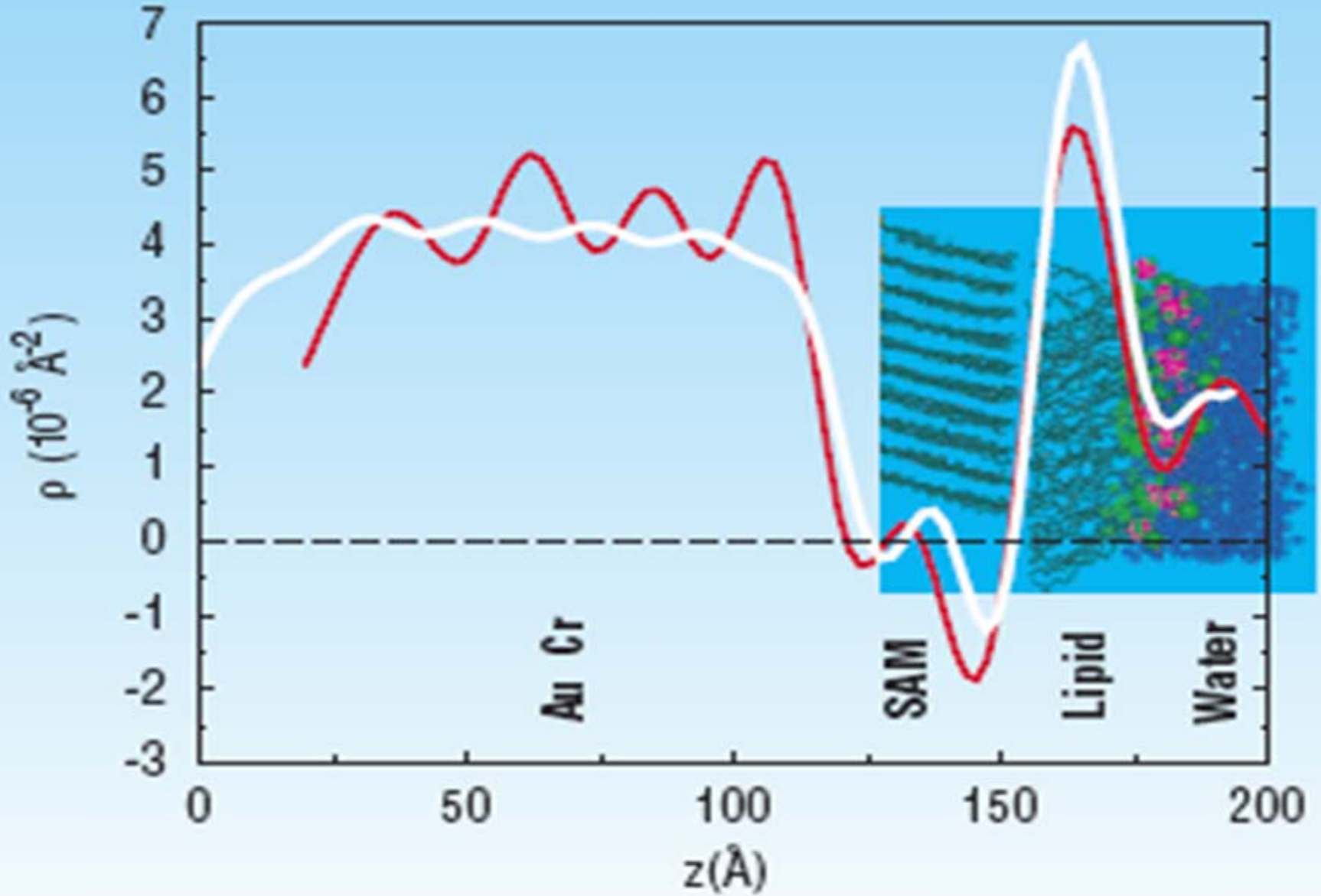
7
6
5
4
3
2
1
0
-1
-2
-3
ρ (10⁻⁶ Å⁻²)
0
50
100
150
200
z(Å)
Au
Cr
SAM
Lipid
Water

UNIQUE DETERMINATION OF BIOMIMETIC MEMBRANE PROFILES BY NEUTRON REFLECTIVITY

New biomimetic membrane materials, of fundamental importance in understanding such key biological processes as molecular recognition, conformational changes, and molecular self-assembly, can be characterized using neutron reflectometry. In particular, scattering length density (SLD) depth profiles along the normal to the surface of a model biological bilayer, which mimics the structure and function of a genuine cell membrane, can be deduced from specular neutron reflectivity data collected as a function of wavevector transfer Q. Specifically, this depth profile can be obtained by numerically fitting a computed to a measured reflectivity. The profile generating the best fitting reflectivity curve can then be compared to cross-sectional slices of the film's chemical composition predicted, for example, by molecular dynamics simulations [1]. However, the uniqueness of a profile obtained by conventional analysis of the film's reflectivity alone cannot be established definitively without additional information. In practice, significantly different SLD profiles have been shown to yield calculated reflectivity curves with essentially equivalent goodness-of-fit to measured data [2], as illustrated in Fig. 1.

The existence of multiple solutions, only one of which can be physical, is especially problematic in cases where a key additional piece of structural or compositional information is lacking as can happen in the investigation of these biological membrane systems.

Why this inherent uncertainty? The neutron specular reflection amplitude for a model SLD can be computed exactly from first principles; the square of its modulus gives the measurable reflectivity. It is firmly established, however, that the complex amplitude is necessary and sufficient for a unique solution of the inverse problem, that of recovering the SLD from reflection measurements. Unambiguous inversion requires both the magnitude and phase of reflection. Once these are known, practical methods [3] exist for extracting the desired SLD.

In fact, considerable efforts were made about a quarter century ago to solve the analogous "phase problem" in X-ray crystallography using known constraints on the scattering electron density [4] and by the technique of isomorphic substitution [5]. Variations of the latter approach have been applied to reflectivity, using a known reference layer in a composite film in place of atomic substitutions. These

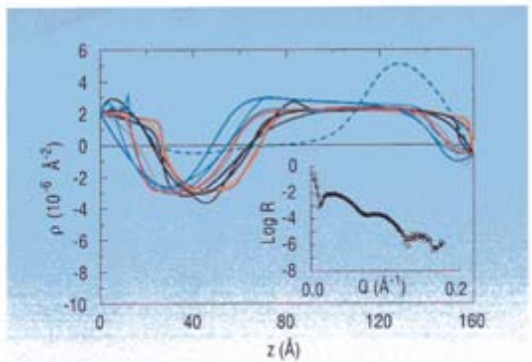

FIGURE 1. Family of scattering length density profiles obtained by model-independent fitting of the reflectivity data in the inset. The profile represented by the blue dashed line is unphysical for this Ti/TiO film system yet generates a reflectivity curve that fits the data with essentially equivalent goodness-of-fit (all the reflectivity curves corresponding to the SLD's shown are plotted in the inset but are practically indistinguishable from one another).

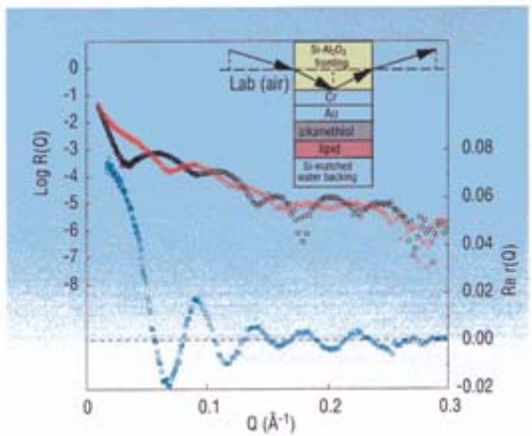

FIGURE 2. Reflectivity curves for the thin film system depicted schematically in the inset, one for a Si fronting (red triangles), the other for Al_2O_3 (black circles). The curve in the lower part of the figure (blue squares) is the real part of the complex reflection amplitude for the films obtained from the reflectivity curves by the method described in the text.

C. F. Majkrzak, N. F. Berk, S. Krueger, J. A. Dura
NIST Center for Neutron Research
National Institute of Standards and Technology
Gaithersburg, MD 20899-8562

C. W. Meuse, V. Silin, J. Woodward, A. L. Plant
NIST Biotechnology Division
National Institute of Standards and Technology
Gaithersburg, MD 20899-8311

M. Tarek
Department of Chemistry
University of Pennsylvania
Philadelphia, PA 19103

solution methods, however, were tied to the Born approximation, which generally is valid in crystal structure determination but which fails catastrophically at low Q (low glancing angles) in reflection from slab-shaped samples such as thin films. Exact inversion requires accurate knowledge of the reflection amplitude over the entire Q-range, especially at low Q.

In this decade the reflection phase problem has been exactly solved using a protocol of three reflectivity measurements on composite films consisting of the film of interest in intimate contact with each of three known reference layers [6, 7]. Subsequently, variations using only two measurements have been shown to partially solve the phase problem, an additional procedure being required to choose between two solution branches, only one of which is physical [8, 9]. In the past year [10], an exact solution has been found for a two measurement strategy in which the film surround, either the fronting (incident) or backing (transmitting) medium, is varied. This new approach is simpler to apply than reference layer methods and is adaptable to many experiments. Surround variation neutron reflectometry has been successfully applied to the challenging type of biological membrane depth profiling described earlier.

In Fig. 2 are plotted a pair of neutron reflectivity curves measured for the layered film structure schematically depicted in the upper right inset, one with Si and the other with Al_2O_3 as the fronting medium. The lower part of Fig. 2 shows the real part of the complex reflection amplitude for the multilayer as extracted from the reflectivity data, according to the method described above, and which was subsequently used to perform the inversion to obtain the SLD shown in Fig. 3. For comparison, the SLD predicted by a molecular dynamics simulation is also shown in Fig. 3, in a slightly distorted version, corresponding to a truncated reflectivity data set, which indicates the spatial resolution of an SLD obtainable in practice. This latter SLD was obtained by inversion of the reflection amplitude computed for the exact model SLD, but using values only up to the same maximum Q value (0.3 $Å^{-1}$) over which the actual reflectivity data sets were collected. Overall, agreement between the experimentally determined profile and the theoretical prediction is remarkable, essentially limited only by the Q-range of the measurement. Surround variation neutron reflectivity thus makes it possible to measure complicated thin film structures without the ambiguity associated with curve fitting. The veridical SLD profile is obtained directly by a first principles inversion.

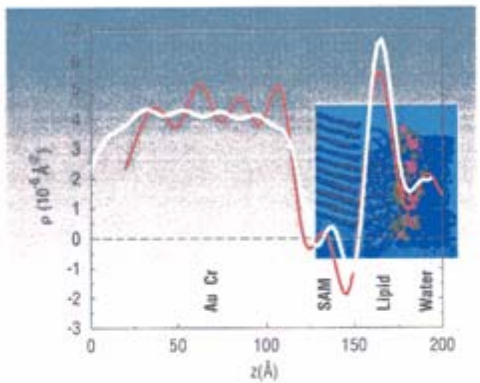

FIGURE 3. SLD profile (red line) resulting from a direct inversion of the Re r of Fig. 2 compared with that predicted by a molecular dynamics simulation (white line) as discussed in the text. The headgroup for the Self-Assembled-Monolayer (SAM) at the Au surface in the actual experiment was ethylene oxide and was not included in the simulation but, rather, modelled separately as part of the Au. Also, the Cr-Au layer used in the model happened to be 20 Å thicker than that actually measured in the experiment.

REFERENCES:

[1] M. Tarek, K. Tu, M.L. Klein, and D. J. Tobias, Biophys. J. **77**, 964 (1999).
[2] N. F. Berk and C. F. Majkrzak, Phys. Rev. B **51**, 11296 (1995).
[3] P. E. Sacks, Wave Motion **18**, 21 (1993).
[4] H. A. Hauptman, Science **233**, 178 (1986).
[5] J. M. Cowley, *Diffraction Physics*, 2nd Ed., (North Holland, Amsterdam, 1990), p. 131.
[6] C. F. Majkrzak and N. F. Berk, Phys. Rev. B **52**, 10825 (1995).
[7] V.O. deHaan, A. A. van Well, S. Adenwalla, and G.P. Felcher, Phys. Rev. B **52**, 10830 (1995).
[8] T. Aktosun and P. E. Sacks, Inverse Problems **14**, 211 (1998).
[9] C. F. Majkrzak and N. F. Berk, Physica B **267-268**, 168 (1999).
[10] C. F. Majkrzak and N. F. Berk, Phys. Rev. B **58**, 15416 (1998).

REFERENCES

* Optics, 3rd Ed., by E.Hecht, Addison Wesley, 1998.

* Neutron Optics, by V.F.Sears, Oxford University Press, 1989.

* Principles of Optics, 6th Ed., by M.Born and E.Wolf, Pergamon Press, 1987.

* Quantum Mechanics, 2nd Ed., by E.Merzbacher, Wiley, 1970.

* Magnetic Multilayers, Ed. by L.H.Bennett and R.E.Watson; article on "Neutron and X-Ray Diffraction Studies of Magnetic Multilayers" by C.F.Majkrzak, J.F.Ankner, N.F.Berk, and D.Gibbs, World Scientific, 1994, p.299 (contains introductory material on neutron and x-ray reflectometry not specific to magnetic materials alone)

* Neutron Reflectometry Studies of Thin Films and Multilayered Materials, C.F.Majkrzak, Acta Physica Polonica A 96, 81(1999) -- this article can also be found at the website: http://www.ncnr.nist.gov -- along with some additional information on analysing neutron reflectivity data (click on "Summer School Course Materials")

“Structural Investigations of Membranes in Biology by Neutron Reflectometry”, C.F.Majkrzak, N.F.Berk, S.Krueger, and U.A.Perez-Salas, Chapter 12 in *Neutron Scattering in Biology*, Edited by J.Fitter, T.Gutberlet, and J.Katsaras, (Springer, Berlin, 2006) p.225-263.

“Polarized Neutron Reflectometry”, C.F.Majkrzak, K.V.O'Donovan, and N.F.Berk, Chapter 9 in *Neutron Scattering from Magnetic Materials*, Edited by T.Chatterji, (Elsevier, Amsterdam, 2006) p.397-471.

“Phase-Sensitive Neutron Reflectometry”, C.F.Majkrzak, N.F.Berk, and U.A.Perez-Salas, *Langmuir* **19**, 7796 – 7810 (2003).